

State-Space Modeling of Viscous Unsteady Aerodynamic Loads

Haithem E. Taha* and Amir S. Rezaei University of California, Irvine, Irvine, California 92697

https://doi.org/10.2514/1.J060956

In this paper, we summarize our recently developed viscous unsteady theory, which couples potential flow with the triple-deck boundary-layer theory. This approach provides a viscous extension of potential-flow unsteady aerodynamics. As such, a Reynolds-number-dependent transfer function is determined for unsteady lift. We then use the Wiener-Hammerstein structure to develop a finite-dimensional approximation of such an infinitedimensional theory, presenting it in a state-space model. This novel nonlinear state-space model of viscous unsteady aerodynamic loads is expected to serve aerodynamicists better than the classical Theodorsen's model because it captures viscous effects (that is, Reynolds number dependence) as well as nonlinearity and additional lag in the lift dynamics; it also allows simulation of arbitrary time-varying airfoil motions (not necessarily harmonic). Moreover, being in a state-space form makes it quite convenient for simulation and coupling with structural dynamics to perform aeroelasticity, flight dynamics analysis, and control design. We then develop a linearization of such a model, which enables analytical results. Subsequently, we derive an analytical representation of the viscous lift frequency response function: an explicit function of both the frequency and Reynolds number. We also develop a state-space model of the linearized response. We finally simulate the nonlinear and linear models to a nonharmonic small-amplitude pitching maneuver at a Reynolds number of 100,000 and compare the resulting lift and pitching moment with those obtained from potential flow; this is in reference to relatively higher-fidelity computations of the unsteady Reynolds-averaged Navier-Stokes equations.

		Nomenclature	L, M_0	=	vi
$(A_P, B_P, C_P, D$	$_{P})$ =	state-space representation of the potential-	L_C, L_{OS}	=	ci
4		flow lift dynamics	L_P, M_{0_P}	=	pc
A_{lpha}	=	pitching amplitude	$_{D_{p}},m_{0_{p}}$		th
a	=	chordwise distance from the midpoint to	$m_{ m v}$	=	vi
		the hinge point, normalized by the half-	P	=	un
		chord	P_s	=	ste
a_j	=	coefficients in the Glauert series expansion	P_{∞}	=	fre
		of the inviscid pressure distribution	$\stackrel{\scriptstyle r}{R}^{\infty}$	=	Re
$a_{0_{ m v}}$	=	leading-edge suction coefficient due to the	$\Re(.)$	=	re
D		viscous correction to Kutta's circulation	s s	=	nc
B_e	=	equivalent scaled trailing-edge singularity	t	=	tir
D		for the triple-deck theory	U	=	fre
B_{e_0}	=	Its value (0.53) of B_e at zero angle of attack	и	=	co
B_s	=	steady trailing-edge singularity	v	=	aiı
$B_{ m v}, ilde{B}_{ m v}$	=	unsteady trailing-edge singularity (viscous	· ·		iti
		correction) and its nondimensional value	$v_{1/2}, v_{3/4}$	=	aiı
b	=	half-chord	01/2, 03/4		m
C(k)	=	Theodorsen function (lift deficiency func-	x, \hat{x}	=	co
		tion or lift frequency response function)	ж, ж		nc
C_L, C_D	=	lift and drag coefficients	y	=	co
C_{L_C}	=	circulatory lift coefficient	y_P	=	ou
$C_{ m v}$	=	viscous lift frequency response function	JP		tei
G(p)	=	transfer function of a linear dynamical sys-	α	=	an
		tem in the Laplace domain	a		(p
$H_n^{(m)}$	=	Hankel function of <i>m</i> th kind of order <i>n</i>	$lpha_e$	=	eq
h, H	=	plunging displacement (positive upward)	α_e		tri
		and its amplitude	$lpha_{ m eff}$	=	vi
i	=	$\sqrt{-1}$	$\alpha_{ m eff}$	=	ste
k	=	reduced frequency	$\alpha_{3/4}$	_	lo
		•	3/4	_	ch

Presented as Paper 2021-1830 at the AIAA Scitech 2021 Forum, Virtual
Event, 11-15 and 19-21 January 2021; received 31 May 2021; revision
received 11 September 2021; accepted for publication 13 September 2021;
published online 1 December 2021. Copyright © 2021 by the American
Institute of Aeronautics and Astronautics, Inc. All rights reserved. All requests
for copying and permission to reprint should be submitted to CCC at www.
copyright.com; employ the eISSN 1533-385X to initiate your request. See
also AIAA Rights and Permissions www.aiaa.org/randp.

^{*}Associate Professor, Mechanical and Aerospace Engineering. Senior Member AIAA.

I_0	=	viscous	lift	and	pitching	moment	at	the
		midchor	d no	nint				

L_C, L_{QS}	=	circulatory and quasi-steady lift
$L_{\rm B} M_{\rm O}$	=	potential-flow lift and pitching m

1 · Op			_	
		the midchord point		
m	=	viscous added mass		

P	=	unsteady pressure distribution
P_s	=	steady pressure distribution
P_{∞}	=	freestream pressure

R = Reynolds number

$$\Re(.)$$
 = real part of its complex argument
s = nondimensional Laplace variable

t	= time variable
U	= freestream velocity
и	= control inputs for a dynamical system

		itive upward)	4
$v_{1/2}, v_{3/4}$	=	airfoil velocities normal to the surface	e at the

midchord and three-quarter-chord points

$$\hat{x}$$
 = coordinate along the airfoil chord and its

$$y_P$$
 = output of the potential-flow dynamical system: the unsteady $v_{3/4}$

$$\alpha_e$$
 = equivalent scaled angle of attack for the triple-deck theory (0–0.47)

$lpha_{ m eff}$	=	viscous unsteady effective angle of attack
α	_	steady angle of attack

α_{s}	_	steady angle of attack
$\alpha_{3/4}$	=	local angle of attack at the three-quarter-

 $[\]Gamma_{\rm v}$ = viscous correction to Kutta's circulation

 ω

[†]Postdoctoral Fellow, Mechanical and Aerospace Engineering. Member AIAA.

 $[\]epsilon$ = small parameter for perturbation analysis θ = tangential angular coordinate along the air-

foil (or plate) chord

= Blasius skin-friction coefficient (0.332)

 $[\]lambda$ = Blasius skin-friction coefficient (0.332) ρ = air density

⁼ an density
= nondimensional time
b = Wagner function

vector of state variables of a dynamical system

⁼ angular frequency of the harmonic motion, rad/s

I. Introduction

THE theory of two-unnensional united by long history that extends for a century. Perhaps the first formal The HE theory of two-dimensional unsteady aerodynamics has a efforts were those of Prandtl [1] and Birnbaum [2] in 1924, considering incompressible, slightly viscous flows around thin airfoils with sharp trailing edges. The key concept is that the flow nonuniformity leads to vorticity generation that emanates at the sharp trailing edge and freely sheds behind the airfoil. In addition, the flow outside these sheets can be considered inviscid. As such, for example, the law of zero total circulation (a consequence of the conservation of angular momentum in inviscid flows) can be used. These assumptions alone are not enough to determine a unique solution for the wing and wake circulations. Then, the Kutta-Zhukovsky condition (smooth flow off the sharp trailing edge) comes to play an essential role in the problem closure. That is, no flow around the sharp edge; hence, the velocity has to be finite at the edge. Finally, in order to obtain an analytical explicit solution to the governing dynamics (the Laplace equation in the velocity potential in this case), one more assumption is usually adopted: assuming small disturbance to the mean flow so that the vorticity sheet shed by the mean flow velocity (flat wake assumption) completes the framework of the classical theory. In summary, the classical theory of unsteady aerodynamics is based on replacing the airfoil and the wake by vorticity distributions (singularities) that satisfy the Laplace equation everywhere in the flowfield, except at the surface of singularities. Three main conditions are applied: 1) nopenetration boundary condition (fluid velocity is parallel to the wing surface), 2) the Kutta condition (smooth flow off the sharp trailing edge), and 3) the conservation of total circulation $((D\Gamma/Dt) = 0)$. This formulation along with the flat wake assumption constitute the classical theory of unsteady aerodynamics.

The aforementioned formulation of the classical theory of unsteady aerodynamics was extensively used throughout the years. In 1925, Wagner [3] used this formulation to solve the indicial problem (lift response due to a step change in the angle of attack). In 1935, Theodorsen [4] used the same formulation to solve the frequency response problem (steady-state lift response due to harmonic oscillation in the angle of attack). In 1938, von Kármán and Sears [5] provided a more general and elaborate representation of the classical formulation, which is of hitherto importance in developing extensions of the classical theory [6,7]. Also, the efforts of Küssner [8] on the sharp-edged gust problem, Schwarz [9] on the frequency response problem, Sears [10] on the sinusoidal gust problem, and Loewy [11] on the returning wake problem are worth mentioning. It should be noted that although the approaches within this framework may be different (i.e., different order of application of the boundary conditions and assumptions as well as different means of calculating the loads), these results are exactly equivalent. For example, Garrick [12] showed that the Theodorsen function and the Wagner function form a Fourier transform pair.

It should be pointed out that even with the several simplifying assumptions mentioned earlier in this paper (potential flow, flat wake, the Kutta assumption/condition, etc.), the unsteady lift response of a two-dimensional airfoil is of an infinite-dimensional nature. That is, in a dynamical-systems narrative, the lift transfer function has infinitely many poles [13]. The need for calculating the aerodynamic loads due to arbitrary time variations of the wing motion along with the need for structural and/or dynamic coupling to assess aeroelastic and/or flight dynamic stability problems invoked more compact representations of the lift dynamics than the infinite-dimensional Theodorsen and Wagner responses. Consequently, a number of finite-state approximations to these response functions were developed. Jones [14] and Jones [15] provided a two-state approximation to the Wagner function in the time domain. Vepa [16] introduced the method of Padé approximants to determine finite-state approximations of the Theodorsen function in the frequency domain. Of particular interest to the aeroelasticity and flight dynamics community is the state-space representation developed by Leishman and Nguyen [17] using the convolution integral with Jones approximation to the Wagner step response function. Unlike these finite-state models that are based on approximating the Theodorsen function in the frequency domain or the Wagner function in the time domain, Peters and Karunamoorthy derived state-space models from the basic governing principles using Glauert expansion [18], and Peters et al. derived state-space models from the basic governing principles using the expansion of potential functions [13,19]. In this formulation, the internal aerodynamic states are of physical meaning; they represent the inflow distributions. Although the formulation of Peters [13] is quite neat, it necessitates a relatively large number (eight) of inflow states to provide a good accuracy; whereas two states were shown to be sufficient for this problem. More recently, Brunton and Rowley [20] performed system identification to construct an empirical state-space model for the unsteady lift dynamics from direct numerical simulations at Reynolds number of 100. However, they maintained the structure (low- and high-frequency behavior) of the Theodorsen lift dynamics; we show in the following that such a structure does not represent the viscous lift dynamics at high frequencies and/or low Reynolds numbers. Recent efforts in developing state-space models of unsteady aerodynamic loads include Refs. [21–23].

Having summarized the main results of the classical theory of unsteady aerodynamics, we should emphasize the following point. Insofar as Prandtl's potential-flow formulation [1] is quite useful in serving the community, and even provides the basis for many recent developments [6,7,24-33], it is mainly based on inviscid flow dynamics; no regard can be given to a finite Reynolds number. More important, it is not complete and invokes a closure or auxiliary condition (e.g., the Kutta condition). Thus, the potential-flow formulation cannot alone determine the amount of shed vorticity at the trailing edge, which is a very crucial quantity because it determines the bound circulation over the airfoil (via conservation of circulation), which in turn dictates the generated lift force. The most common auxiliary condition used in literature is the Kutta condition, whose application to steady flows has been very successful. However, its application to unsteady flows has been controversial (see the work of Crighton [34]).

The need for an auxiliary condition alternative to the Kutta condition goes as early as the work of Howarth [35] with a research flurry on the applicability of the Kutta condition to unsteady flows in the 1970s and 1980s [34,36–39]. This research was mainly motivated by the failure to capture an accurate flutter boundary [40-42]. Since flutter simply lies in the intersection between unsteady aerodynamics and structural dynamics, and because the structural dynamics theory is in a much better status (the vibration of slender beams can be accurately predicted using the exact beam theory, for example), it has been deemed that the flaw stems from the classical unsteady aerodynamic theory (particularly the Kutta condition), as suggested by Chu [43] and Shen and Crimi [44], among others. Moreover, since these deviations occurred even at a zero angle of attack (or lift) [45,46], it was inferred that there is a fundamental issue with such a theory that is not merely a higher-order effect due to nonlinearities at high angles of attack [43]. Therefore, there was almost a consensus that the Kutta condition has to be relaxed, particularly at large frequencies, large angles of attack, and/or low Reynolds numbers [38,47,48]. In fact, Orszag and Crow [49] regarded the full Kutta condition solution as "indefensible." Interestingly, this dissatisfaction of the Kutta condition and the need for its relaxation are recently rejuvenated with the increased interests in the low-Reynolds-number high-frequency bioinspired flight [6,50-55]. For more recent discussions about the unsteady Kutta condition, the reader is referred to the efforts of Xia and Mohseni [56], Taha and Rezaei [57], and Zhu et al. [58].

We note that the main concern about the Kutta condition in unsteady flows is because vorticity generation and unsteady lift development may enjoy important viscous effects, which may not be captured in a purely inviscid theory. To resolve this issue, we recently developed a viscous extension of the classical theory of unsteady aerodynamics [57], equivalently, an unsteady extension of the viscous boundary-layer theory. It is based on a special boundary-layer theory (the triple deck [59–61]) that pays close attention to the details in the vicinity of the trailing edge where the Blasius boundary layer [62] interacts with the Goldstein near-wake layer [63]. Our viscous extension resulted in a Reynolds-number-dependent extension of the Theodorsen lift frequency response. It was found that the viscous correction induces a significant phase lag

Downloaded by UNIV CA - IRVINE on May 25, 2022 | http://arc.aiaa.org | DOI: 10.2514/1.J060956

TAHA AND REZAEI 2253

to the circulatory lift component, particularly at low Reynolds numbers and high frequencies, that matches high-fidelity simulations of Navier–Stokes and previous experimental results [39,42,46,64].

In this paper, we summarize the developed viscous unsteady aerodynamic theory. Based on which, we use the Wiener-Hammerstein structure to develop a nonlinear state-space model of the viscous unsteady loads. We then linearize such a theory to determine an analytical representation, extending the Theodorsen lift frequency response function to the viscous case. That is, we provide an analytical lift frequency response function that explicitly depends not only on the reduced frequency but also on the Reynolds number. Similar to the Theodorsen function, this viscous frequency response function is infinite-dimensional (i.e., has infinitely many poles). We then develop a finite-state approximation of this infinite-dimensional viscous frequency response. That is, we provide a linearized state-space model, extending that of Leishman and Nguyen [17] to the viscous case; the Reynolds number appears as a parameter in such a state-space model. These tools will be of paramount importance in coupling viscous unsteady aerodynamics with structural dynamics for aeroelasticity and flight dynamics analysis as well as control synthesis. However, similar to most classical models, the proposed one adopts some simplifying assumptions; Table 1 summarizes these assumptions in comparison to the unsteady models commonly used in the literature.

The specific contributions of this paper are summarized in the following three points:

- 1) Develop a nonlinear state-space model for the viscous unsteady lift and moment on a pitching-plunging flat plate. The Reynolds number R is a parameter in this model.
- 2) Develop a linearized version of the aforementioned nonlinear statespace model; this linear model can be easily combined with structural/ body dynamics for standard linear stability analysis (e.g., flutter).
- 3) Derive *analytical* expressions for the viscous lift frequency response function (i.e., a viscous Theodorsen function) that does not only depend on the reduced frequency but also the Reynolds number.

II. Viscous Theory of Unsteady Aerodynamics

A. Background: The Triple-Deck Boundary-Layer Theory

In the early 1900s, Prandtl formulated the well-known boundarylayer equations [65]: the nonlinear partial differential equations that approximate Navier-Stokes equations in the thin viscous layer around the airfoil. In 1908, Blasius [62] solved this set of equations over a flat plate at a zero angle of attack subject to the no-slip boundary condition on the plate, which led to the celebrated Blasius boundary-layer solution. Later (in 1930), Goldstein [63] solved the same boundary-layer equations of Prandtl in the wake region behind the plate, replacing the no-slip condition with a zero-stress condition on the wake centerline. He found that the removal of the wall accelerates the flow, leading to a favorable pressure gradient. That is, near the trailing edge, there are two boundary layers interacting with each other, as shown in Fig. 1: the Blasius boundary layer, whose thickness is of order $R^{-1/2}$; and the Goldstein near wake, whose thickness is scaled as $R^{-1/2}x^{1/3}$, where R is the Reynolds number and x is the distance downstream of the edge [34]. The triple-deck theory has been devised to model such local interactions near the trailing edge of a flat plate in steady flow. In contrast to the classical boundary-layer theory where only the normal coordinate is scaled, the tangential coordinate is also scaled (zoomed) in the triple-deck theory to resolve such interactions. Scaling dictates that the transition region between the two layers takes place over a short length of order $R^{-3/8}$ (as shown in Fig. 1), which is similar to Lighthill's supersonic shock-wave/boundary-layer interaction [66]. In conclusion, the triple-deck theory represents a solution to the discontinuity of the viscous boundary condition at the edge [67]: from a zero tangential velocity on the airfoil to a zero pressure discontinuity on the wake centerline.

Aerodynamicists modeled this transition through three layers (triple-deck theory): 1) the upper deck, which constitutes an irrotational flow outside of the main boundary layer; 2) the main deck, which is an inviscid layer, although rotational; and 3) the lower deck, which is a viscous sublayer inside the main deck (as shown in Fig. 1), where the full boundary-layer equations apply. Stewartson [59] and Messiter [60] were the first to develop the triple-deck theory for a flat plate in a steady flow at a zero angle of attack.

Brown and Stewartson [61] extended the work of Stewartson [59] and Messiter [60] to the case of a small but nonzero angle of attack α_s in the order of $R^{-1/16}$. This range is of interest because 1) if α_s is much smaller, then the flow can be considered as a perturbation to the case of $\alpha_s = 0$; and 2) if it is much larger, then the flow would separate well before the trailing edge. Over this range, the resulting adverse pressure gradient is of the same order as the favorable pressure

Table 1	Comparison among different assumptions adopted in classical inviscid unsteady models and the proposed
	viscous one, in addition to the applicability of these models

	_	Classical theory [3–5]	Approximations [13–19]	Vortex methods	Proposed model
Assumptions	Small disturbance	×	×		×
	Flat wake	×	×		×
	Kutta condition	×	×	×	
Applications	Arbitrary kinematics		✓	✓	√
	State space		✓		\checkmark
	R effect				✓

A cross indicates an assumption (i.e., weakness) in the model, while a a check indicates an applicability of the model to the point of concern (i.e., strength).

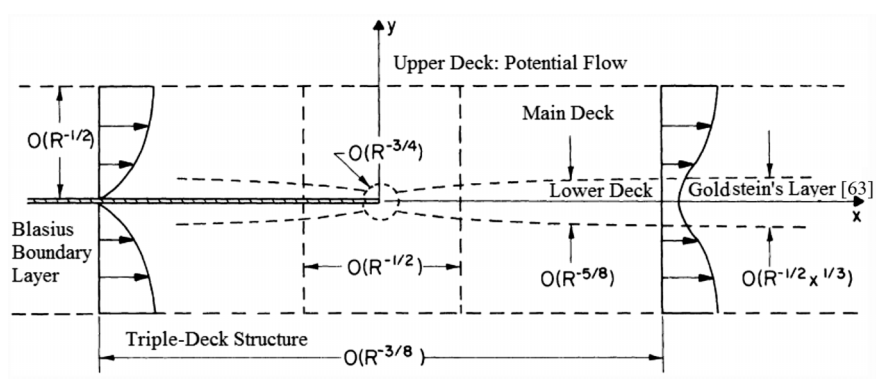


Fig. 1 Triple-deck structure and various flow regimes. Adapted from the work of Messiter [60].

gradient in the triple deck, leading to separation in the immediate vicinity of the trailing edge, which is called *trailing-edge stall*. Brown and Stewartson [61] formulated such a problem and showed that the flow in the lower deck is governed by partial differential equations that are solved numerically for each value of $\alpha_e = R^{1/16} \lambda^{-9/8} \alpha_s$, where $\lambda = 0.332$ is the Blasius skin-friction coefficient. Chow and Melnik [68] solved the triple-deck boundary-layer equations in the case of $0 < \alpha_e < 0.45$ and concluded that the flow will separate from the suction side of the airfoil from the trailing edge at $\alpha_e = 0.47$ (trailing-edge stall angle). We remark that this α_e value for trailing-edge stall corresponds to quite a small value for the actual angle of attack: $\alpha = 3.1-4.2$ deg for $R = 10^4-10^6$.

Setting the axes at the center of the plate $(-1 \le \hat{x} \le 1)$ on the plate), Brown and Stewartson [61] wrote the steady pressure distribution near the trailing edge $(\hat{x} = 1)$ as

$$P_s(\hat{x} \to 1) = \rho U^2 \left[-\alpha_s \sqrt{\frac{1-\hat{x}}{2}} + \frac{B_s/2}{\sqrt{\frac{1-\hat{x}}{2}}} \right] \operatorname{sgn}(y) \tag{1}$$

where ρ is the fluid density; U is the freestream; $\operatorname{sgn}(y)$ is positive on the upper surface; α_s is the steady angle of attack; and B_s is the steady trailing-edge singularity term, which is supposed to be zero according to the Kutta condition. In contrast, it is determined by matching the triple deck with the outer flow. The numerical solution by Chow and Melnik [68] provides B_e as a nonlinear function of α_e , which is represented here in Fig. 2a, where

$$\alpha_e = \alpha_s e^{-1/2} \lambda^{-9/8}$$
 and $B_s = 2e^3 \lambda^{-5/4} B_e(\alpha_e) \alpha_s$ (2)

where α_s and α_e are in radians, and $\epsilon = R^{-1/8} \ll 1$ [59]. In other words, Fig. 2a and Eq. (2) provide the trailing-edge singularity B_s as a nonlinear function of the angle of attack α_s in a steady flow. Based on this theory, the Kutta steady lift can be corrected as

$$C_L = 2\pi(\sin\alpha_s - B_s) \tag{3}$$

which results in the viscous lift shown in Fig. 2b at different Reynolds numbers.

B. Viscous Unsteady Lift Frequency Response Using Triple-Deck Theory

Brown and Daniels [67] were the first to extend the steady tripledeck theory to the case of an oscillatory pitching flat plate. Unlike the steady case, there is a Stokes layer near the wall that is of order $\sqrt{\nu/\omega}$, where the viscous term is balanced by the time-derivative term in the equations. Brown and Daniels considered the impractical yet mathematically appealing case of very high-frequency $k = O(R^{1/4}) =$ $1/e^2$ and very small-amplitude $O(R^{-9/16})$, where k is the reduced frequency. Luckily, focusing on the more practical case of $0 < k \ll$ $Re^{1/4}$ and $\alpha = O(R^{-1/16})$ results in vanishing the time-derivative term in both the main deck and lower deck equations, as shown by Brown and Cheng [69]. Therefore, the boundary-layer equations look the same as those governing the steady case at a nonzero α_s (studied by Brown and Stewartson [61]) with a proper definition for the equivalent steady angle of attack. However, we emphasize that this approach is not a quasi-steady solution; although the time derivative does not show up in the lower deck equations, the correspondence with the steady equations implies an equivalent angle of attack that is dependent on the oscillation frequency, as will be shown in the following. Therefore, the lower deck system is dynamical (i.e., possesses a nontrivial frequency response).

In our recent efforts [57,70], we have developed a viscous extension of the classical theory of unsteady aerodynamics using the triple-deck boundary-layer theory discussed earlier in this paper. For an arbitrarily deforming thin airfoil in the presence of a uniform stream U, the inviscid pressure distribution is typically written as [71–73]

$$P(\theta, t) - P_{\infty} = \rho \left[\frac{1}{2} a_0(t) \tan \frac{\theta}{2} + \sum_{n=1}^{\infty} a_n(t) \sin n\theta \right]$$
 (4)

where θ is the tangential angular coordinate along the plate (zero at the trailing edge, and π at the leading edge). Each term in the series of Eq. (4) automatically satisfies the Kutta condition (zero loading at the trailing edge). The pressure on the lower side is given by the negative of Eq. (4). The no-penetration boundary condition provides a means to determine all the coefficients a_n (except a_0) in terms of the plate motion kinematics, as shown by Robinson and Laurmann (Ref. [73] p. 491). For example, for a pitching–plunging flat plate, as shown in Fig. 3, the normal velocity of the plate is written as

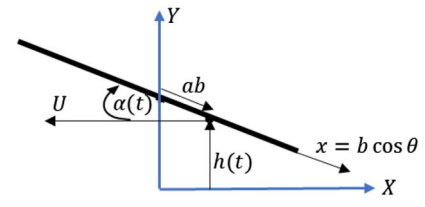
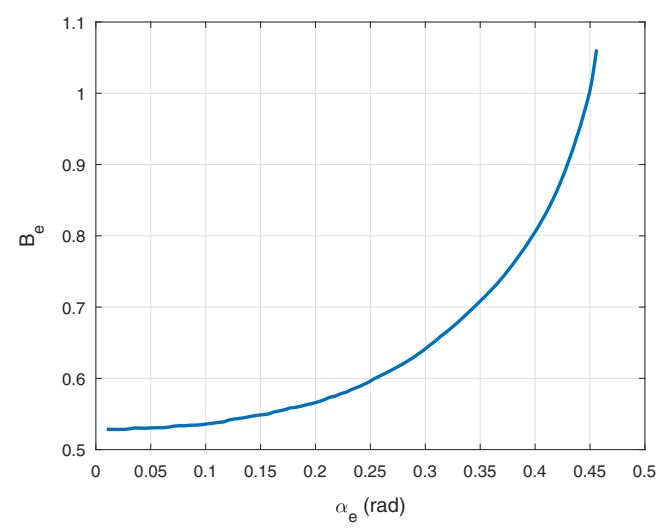
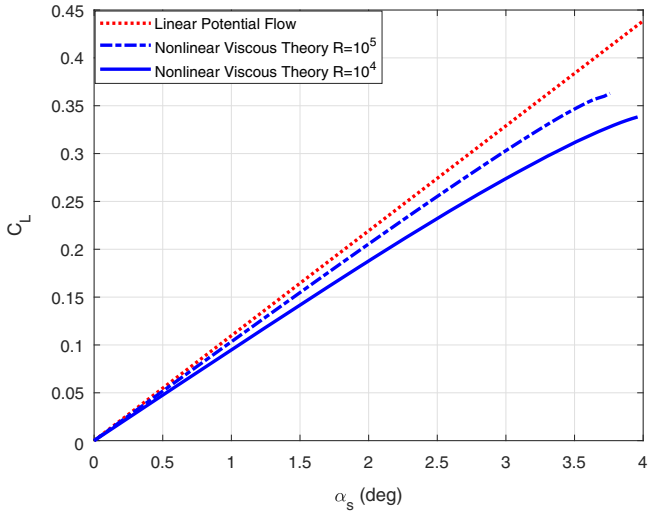


Fig. 3 Schematic diagram for an oscillating flat plate.



a) Numerical solution of $B_e = B_e (\alpha_e)$



b) C_L vs α

Fig. 2 Chow and Melnik numerical solution of the steady lower deck equations for $0 < \alpha_e < 0.45$ [68] and the corresponding nonlinear viscous steady $C_L - \alpha$ curve at different Reynolds numbers.

$$v(x,t) = \dot{h}(t)\cos\alpha(t) - \dot{\alpha}(t)(x-ab) - U\sin\alpha(t),$$

$$-b \le x \le b$$
 (5)

where b is the half-chord length, h is the plunging displacement (positive upward), α is the pitching angle (angle of attack, positive pitching up), and ab represents the chordwise distance from the midpoint to the hinge point, as shown in Fig. 3. This type of kinematics results in

$$a_1(t) = b(\dot{v}_{1/2}(t) - U\dot{\alpha}(t)), \quad a_2(t) = -\frac{b^2\ddot{\alpha}(t)}{4}, \quad \text{and}$$

$$a_n = 0 \quad \forall \ n > 2$$
(6)

where $v_{1/2}$ is the normal velocity at the midchord point, which is given by

$$v_{1/2}(t) = \dot{h}(t)\cos\alpha(t) + ab\dot{\alpha}(t) - U\sin\alpha(t)$$

The determination of a_0 (leading-edge singularity term) is more involved in the sense that it requires solving an integral equation, which cannot be solved analytically for arbitrary time-varying wing motion. It has been solved for some common inputs, e.g., step change in the angle of attack resulting in the Wagner response [3], simple harmonic motion resulting in Theodorsen's frequency response [4], sharp-edged gust resulting in Küssner's function [8], and sinusoidal gust resulting in Sears's function [10]. For example, the harmonic solution of Theodorsen implies [73]

$$a_0 = U[2v_{3/4}C(k) + b\dot{\alpha}] \tag{7}$$

where $v_{3/4}$ is the normal velocity at the three-quarter-chord point; and C(k) is the Theodorsen frequency response function, which depends on the reduced frequency $k = \omega b/U$ as

$$C(k) = \frac{H_1^{(2)}(k)}{H_1^{(2)}(k) + iH_0^{(2)}(k)}$$
(8)

where $H_n^{(m)}$ is the Hankel function of the *m*th *m*th kind of order *n*. Finally, the potential-flow lift force and pitching moment (positive pitching up) at the midchord point are written as

$$L_P = -\pi \rho b(a_0 + a_1)$$
 and $M_{0_P} = \frac{\pi}{2} \rho b^2 (a_2 - a_0)$ (9)

In the common classification proposed by Theodorsen [4], the terms proportional to C(k) represent the circulatory contribution; whereas the other *algebraic* terms (i.e., free of dynamic lag), which are proportional to acceleration, represent the noncirculatory contribution [74].

Relaxing the Kutta condition is equivalent to introducing an additional circulation $\Gamma_{\rm v}$ beyond Kutta's. If the problem is formulated using conformal mapping (i.e., mapping a circular cylinder to a flat plate), this vortex is introduced at the center of the cylinder, which induces singularities at the trailing and leading edges of the plate. Clearly, this circulation is of unknown strength; there is no means within potential flow for its determination. The Kutta condition dictates that it must vanish so as to remove the singularity at the trailing edge. However, we relax the Kutta condition and determine its dynamics via matching with the triple-deck boundary-layer theory. This additional circulation modifies the inviscid unsteady pressure distribution [Eq. (4)] as

$$P(\theta, t) - P_{\infty} = \rho \left[\frac{1}{2} a_0(t) \tan \frac{\theta}{2} + \sum_{n=1}^{\infty} a_n(t) \sin n\theta + \frac{1}{2} B_{\nu}(t) \left(\cot \frac{\theta}{2} + a_{0\nu}(t) \tan \frac{\theta}{2} \right) \right]$$
(10)

where the correction $B_{\rm v}$ is related to the additional circulation as $B_{\rm v}=(U\Gamma_{\rm v}/2\pi b)$, and $a_{0_{\rm v}}$ is the leading-edge singularity due to $\Gamma_{\rm v}$. This term has a nontrivial dynamics (there is a nontrivial transfer function from $\Gamma_{\rm v}$ to $a_{0_{\rm v}}$). It can be determined from potential-flow considerations: it is the a_0 term in the unsteady inviscid pressure distribution Eq. (4) over the plate due to a bound circulation $\Gamma_{\rm v}$, ignoring the quasi-steady contribution (i.e., the wake effects only). Therefore, similar to the general a_0 term, it cannot be determined analytically for arbitrary kinematics; there is an analytical expression in the special case of harmonic motion ($a_{0_{\rm v}}=2C(k)-1$ [69]). In our recent effort [57], we used the unsteady triple-deck theory, exploiting the vanishing of the time-derivative term from the boundary-layer equations to determine $B_{\rm v}$ in terms of k and k. Then, the viscous unsteady lift and pitching moment will be written as

$$L = -\pi \rho b (a_0 + a_1 + B_v (1 + a_{0_v})) \quad \text{and}$$

$$M_0 = \frac{\pi}{2} \rho b^2 (a_2 - a_0 + B_v (1 - a_{0_v})) \tag{11}$$

To determine the viscous correction B_v of the pressure distribution, consider approaching the trailing edge $(\theta \to 0 \text{ or } \hat{x} = (x/b) \to 1)$, the pressure distribution [Eq. (10)] is then written as

$$P(\hat{x} \to 1; t) - P_{\infty} = \rho \left[\left(\frac{1}{2} a_0(t) + 2 \sum_{n=1}^{\infty} n a_n(t) + \frac{1}{2} B_{v}(t) a_{0_{v}}(t) \right) \sqrt{\frac{1 - \hat{x}}{2}} + \frac{B_{v}(t)/2}{\sqrt{\frac{1 - \hat{x}}{2}}} \right]$$
(12)

which has the same form as the steady distribution given in Eq. (1) with the equivalence

$$\alpha_{s}(t) \equiv \frac{1}{U^{2}} \left| \frac{1}{2} a_{0}(t) + 2 \sum_{n=1}^{\infty} n a_{n}(t) \right| \quad \text{and}$$

$$B_{v}(t) \equiv B_{s} = -2\epsilon^{3} \lambda^{-5/4} \left(\frac{1}{2} a_{0}(t) + 2 \sum_{n=1}^{\infty} n a_{n}(t) \right) B_{e}(\alpha_{e}) \quad (13)$$

where α_s and B_s are the equivalent steady angle of attack and the trailing-edge singularity term, respectively. Note that the negligence of the term $B_v a_{0_v}$ when performing such an equivalence was justified in our earlier effort [57]. This comparison along with the fact that the time-derivative term does not enter the triple-deck equations is suggestive to use the steady solution by Chow and Melnik [68] of the inner deck equations for the unsteady case with the equivalence shown earlier in this paper, which is valid in the range $0 < k < O(R^{1/4})$. In the aforementioned equivalence, if the term

$$\frac{1}{2}a_0(t) + 2\sum_{n=1}^{\infty}na_n(t)$$

is negative, then the top of the oscillating plate will correspond to the top of the steady plate; if it is positive, then the top of the oscillating plate should correspond to the bottom of the steady one. In either case, α_s would be positive.

For a harmonically oscillating flat plate at a given reduced frequency k and Reynolds number R, the coefficients a_0 , a_1 , and a_2 of the inviscid pressure distribution are given in Eqs. (6) and (7). Thus, α_s can be obtained accordingly from Eq. (13). Care should be taken when applying Eq. (13). It should be applied instantaneously: at each time instant, the right-hand side containing the a coefficients is complex because a_0 contains the complex-valued function C(k). The instantaneous $\alpha_s(t)$ should be given by

$$\alpha_s(t) = \frac{1}{U^2} \left| \Re \left[\frac{1}{2} a_0(t) + 2a_1(t) + 4a_2(t) \right] \right|$$

where $\Re(.)$ denotes the real part of its complex argument. As such, the equivalent angle of attack $\alpha_e(t)$ for the numerical solution of Chow and Melnik [68] is obtained from Eq. (2) with $\epsilon=R^{-1/8}$. Note that if $\alpha_e(t)$ exceeds 0.47, then the simulation should be terminated because such a value implies trailing-edge stall; beyond which, the current analysis is not valid. Using Fig. 2a, one can obtain $B_e(t)$, which in turn is substituted in Eq. (13) to determine the viscous correction $B_v(t)$. Finally, the unsteady viscous lift and moment are written as

$$L = \underbrace{\frac{-\pi\rho b^2 \dot{v}_{1/2}}{\text{Noncirculatory}}}_{\text{Potential Flow Solution } L_P} \underbrace{\frac{-2\pi\rho U b v_{3/4} C(k)}{\text{Circulatory}}}_{\text{Circulatory}} - \underbrace{\frac{2\pi\rho b B_{\text{v}} C(k)}{\text{Viscous Correction}}}_{\text{Viscous Correction}}$$
(14)

This equation implies that the viscous contribution to the lift appears as a correction to the angle of attack $\alpha_{3/4} = -v_{3/4}/U$ at the three-quarter-chord point by an amount of $\tilde{B}_{\rm v} = (B_{\rm v}/U^2)$. That is, the viscous unsteady circulatory lift coefficient can be written as $C_{L_C} = 2\pi(\alpha_{3/4} - \tilde{B}_{\rm v})C(k)$. Also, the pitching moment at the midchord point can be written as

$$M_{0} = -\pi \rho b^{2} \left[\underbrace{\frac{b^{2}}{8} \ddot{\alpha} + \frac{b}{2} U \dot{\alpha} + U v_{3/4} C(k)}_{\text{Potential Flow Solution } M_{0_{p}}} - \underbrace{B_{v} (1 - C(k))}_{\text{Viscous Correction}} \right]$$
(15)

The viscous correction $B_{\rm v}C(k)$ to the unsteady circulatory lift is inherited in the pitching moment as well. However, there is an additional viscous correction to the pitching moment. As can be inferred from Eq. (11), the viscous lift contribution has two components: $B_{\rm v}a_{0_{\rm v}}$ acting at the quarter-chord point, similar to the inviscid circulatory lift; and $B_{\rm v}$ acting at the three-quarter-chord point. Hence, viscosity, not only induces lag to the circulatory lift [57] but also shifts the center of pressure; both effects are expected to impact the flutter boundary [75,76].

III. Nonlinear State-Space Model of Viscous Unsteady Loads

A. Model Development

Similar to the classical potential-flow models of unsteady aerodynamics (e.g., Theodorsen [4]), the aforementioned viscous unsteady model is infinite-dimensional; i.e., the lift transfer function has infinitely many poles. The development of a finite-dimensional approximation of the current infinite-dimensional nonlinear dynamical model may be challenging; the search for a special class/form of nonlinear systems that can fit such an infinite-dimensional model is not trivial. Luckily, the nature of the system, as depicted in the block diagram in Fig. 4, invokes the Wiener-Hammerstein structure as a paradigm model of the viscous unsteady lift dynamics, where a static/algebraic nonlinear function is sandwiched between two linear dynamical systems [77-79], as shown in Fig. 5. Moreover, identification of the Wiener-Hammerstein model parameters (the static nonlinear function and the two linear transfer functions) is straightforward in the current viscous unsteady model. As shown in Fig. 4, the static nonlinear function comes from the steady triple-deck nonlinearity, and the two linear dynamical systems come from the potential-flow lift dynamics. So, we can construct a state-space model for the viscous unsteady loads by using a proper finite-state approximation of such a linear lift dynamics (e.g., Leishman and Nguyen [17] or Peters [13]); see the Appendix for a brief study of different finite-state approximations of the potential-flow lift dynamics.

Let the quadruple (A_P, B_P, C_P, D_P) represent a state-space model of potential-flow lift dynamics [i.e., a state-space representation of C(k)]. Then, the corresponding transfer function must have a high-frequency gain of 1/2, which implies that $D_p = 1/2$ [74]. Also, the corresponding transfer function must have a unity dc gain. That is, if it is fed by, say, $v_{3/4}$, the output would be $v_{3/4}C(k)$ in the time domain (i.e., the unsteady version of $v_{3/4}$). Therefore, we can write

$$\dot{\chi}_1 = [A_P]\chi_1 + [B_P]v_{3/4},$$

$$y_P = [C_P]\chi_1 + [D_P]v_{3/4}$$
(16)

where $\chi_1 \in \mathbb{R}^n$ is the vector of internal aerodynamic states constituting the adopted potential-flow finite-state model of order n. The subscript of 1 is used since another set of potential-flow states will be needed, as will be shown in the following. In this formulation, the output y_p represents $v_{3/4}C(k)$ in the time domain. As such, the potential-flow circulatory aerodynamic loads can be determined directly from y_p according to Eqs. (6)–(9) as

$$\begin{pmatrix} L_P \\ M_{0_P} \end{pmatrix}_C = -\pi \rho U b \begin{pmatrix} 2 \\ b \end{pmatrix} y_P \triangleq U[\mathbb{F}] y_P \tag{17}$$

where \mathbb{F} is the matrix (column) defining such a linear algebraic relation. In addition, the noncirculatory loads can be written in an abstract way as

$$\begin{pmatrix} L_P \\ M_{0_P} \end{pmatrix}_{NC} = [\mathbb{M}] \begin{pmatrix} \ddot{\alpha} \\ \ddot{h} \end{pmatrix} + [\mathbb{C}] \begin{pmatrix} \dot{\alpha} \\ \dot{h} \end{pmatrix} \tag{18}$$

where the matrices \mathbb{M} and \mathbb{C} represent *added* mass and damping (actually, the negative of mass and damping) induced by the non-circulatory loads, which are given by

$$\mathbb{M} = -\pi \rho b^2 \begin{bmatrix} ab & \cos \alpha \\ b^2/8 & 0 \end{bmatrix}, \qquad \mathbb{C} = \pi \rho b^2 \begin{bmatrix} U\cos \alpha & \dot{\alpha}\sin \alpha \\ -Ub/2 & 0 \end{bmatrix}$$
(19)

As such, adding the circulatory and noncirculatory contributions, the total potential-flow aerodynamic loads can be written in an abstract form as

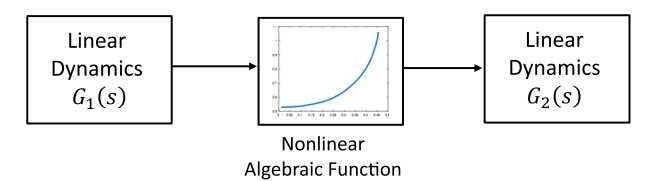


Fig. 5 Wiener-Hammerstein model.

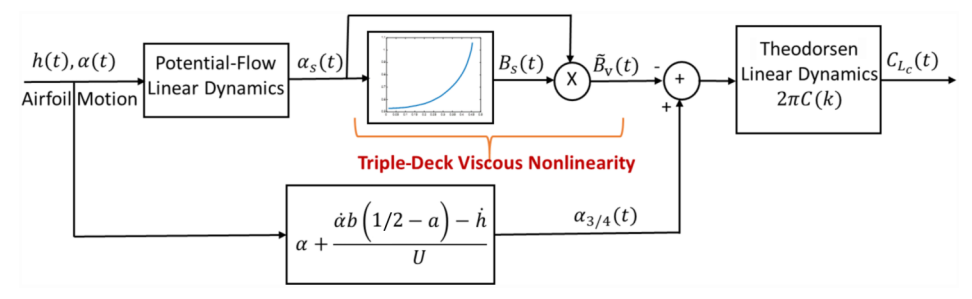


Fig. 4 Block diagram describing the dynamics of the viscous unsteady circulatory lift.

$$\begin{pmatrix} L_P \\ M_{0_P} \end{pmatrix} = [\mathbb{M}] \begin{pmatrix} \ddot{\alpha} \\ \ddot{h} \end{pmatrix} + [\mathbb{C}] \begin{pmatrix} \dot{\alpha} \\ \dot{h} \end{pmatrix} + U[\mathbb{F}] y_P \tag{20}$$

The block diagram shown in Fig. 4 implies that the sought state-space model would include at least double the number n of the states constituting the adopted potential-flow finite-state model because it includes the potential-flow dynamics twice. In addition, to have a proper representation, we consider $\ddot{\alpha}$ and \ddot{h} to be the inputs to the aerodynamical system [80,81]; hence, α , $\dot{\alpha}$, and \dot{h} will be states. That is, the sought state-space model would be of order 2n+3, whose state vector is $\boldsymbol{\chi}=\left[\chi_1,\chi_2,\alpha,\dot{\alpha},\dot{h}\right]^T$ and input vector is $\boldsymbol{u}=\left[\ddot{\alpha},\ddot{h}\right]^T$. As can be concluded from Eqs. (14) and (15), the potential-flow lift given earlier in this paper needs to be corrected by adding terms proportional to B_v and $B_vC(k)$. The latter can be determined by passing the former to the potential-flow state-space representation [Eq. (16)].

To develop a state-space representation for the viscous correction terms B_v and $B_vC(k)$, which is the main contribution of this work, we recall Eq. (13) and define the *effective* angle of attack

$$\alpha_{\text{eff}} = \frac{1}{U^2} \left[\frac{1}{2} a_0(t) + 2 \sum_{n=1}^{\infty} n a_n(t) \right]$$

Note that this $\alpha_{\rm eff}$ is different from the common notion of the effective angle of attack in potential flow. The former is a term special to the developed viscous theory, whereas the latter is simply given by the angle of attack $\alpha_{3/4}$ at the three-quarter-chord point (Ref. [71] p. 80). Based on this definition, the equivalent steady angle of attack is simply given by $\alpha_s = |\alpha_{\rm eff}|$. Then, we use Eqs. (6) and (7) to write $\alpha_{\rm eff}$ as

$$\alpha_{\text{eff}} = \frac{v_{3/4}}{U}C(k) - \frac{3b\dot{\alpha}}{2U} + \frac{2b\dot{v}_{1/2} - b^2\ddot{\alpha}}{U^2}$$
(21)

Realizing that $v_{3/4}C(k)$ is simply y_P , and substituting for $\dot{v}_{1/2}$, we write α_{eff} in terms of the states and inputs:

$$\alpha_{\text{eff}}(\boldsymbol{\chi};\boldsymbol{u}) = \frac{-1}{U} \left[C_P \ b\left(\frac{3}{2} + 2\cos\alpha + D_P\left(\frac{1}{2} - a\right)\right) \frac{2b\dot{\alpha}}{U}\sin\alpha - D_P\cos\alpha \right]$$

$$\begin{pmatrix} \chi_1 \\ \dot{\alpha} \\ \cdot \end{pmatrix} - D_P\sin\alpha + \frac{b}{U^2} \left[(2a - 1)b \ 2\cos\alpha \right] \begin{pmatrix} \ddot{\alpha} \\ \ddot{n} \end{pmatrix}$$
(22)

As can be seen from Eq. (22), the effective angle of attack in the viscous theory depends on the accelerations. So, for relatively fast motion, α_{eff} reaches significant values, which trigger nonlinearity of the $B_e(\alpha_e)$ curve (Fig. 2a), even with small amplitudes.

Having developed a state-space representation of $\alpha_{\rm eff}$ (and consequently α_s), Eq. (13) implies that the viscous correction $B_{\rm v}$ can be written in terms of the states and inputs as

$$B_{v}(\boldsymbol{\chi};\boldsymbol{u}) = -2\epsilon^{3}\lambda^{-5/4}U^{2}\alpha_{\text{eff}}(\boldsymbol{\chi};\boldsymbol{u})B_{e}\left(\epsilon^{-1/2}\lambda^{-9/8}|\alpha_{\text{eff}}(\boldsymbol{\chi};\boldsymbol{u})|\right)$$
(23)

where $B_e(.)$ is a nonlinear function coming from the numerical solution of Chow and Melnik [68] to the triple-deck problem: specifically from Fig. 2a. Finally, the unsteady version of B_v [i.e., $B_vC(k)$] can be written with the aid of the potential-flow finite-state model [Eq. (16)] as

$$\dot{\chi}_2 = [A_P]\chi_2 + [B_P]B_v,$$
 $y_v = [C_P]\chi_2 + [D_P]B_v$ (24)

where y_v simply represents $B_vC(k)$ in the time domain. The total viscous unsteady loads can then be written according to Eqs. (14) and (15) as

$$\begin{pmatrix} L \\ M_0 \end{pmatrix} = \begin{pmatrix} L_P \\ M_{0_P} \end{pmatrix} - \pi \rho b \begin{pmatrix} 2 \\ b \end{pmatrix} B_{\mathbf{v}} C(k) + \pi \rho b^2 \begin{pmatrix} 0 \\ 1 \end{pmatrix} B_{\mathbf{v}}$$
 (25)

where the potential-flow loads

$$\begin{pmatrix} L_P \\ M_{0_P} \end{pmatrix}$$

are given by Eq. (20). Realizing that

$$\mathbb{F} = -\pi \rho b \binom{2}{b}$$

and that $B_vC(k)$ is y_v , which is given by Eq. (24), we finalize the state-space model as follows. The state equation is written as

$$\frac{d}{dt} \begin{pmatrix} \chi_{1} \\ \chi_{2} \\ \alpha \\ \dot{\alpha} \\ \dot{h} \end{pmatrix} = \begin{bmatrix} A_{P} & 0_{n \times n} & 0_{n \times 1} & -B_{P}b \left(\frac{1}{2} - a\right) & B_{P}\cos\alpha \\ 0_{n \times n} & A_{P} & 0_{n \times 1} & 0_{n \times 1} & 0_{n \times 1} \\ 0_{1 \times n} & 0_{1 \times n} & 0 & 1 & 0 \\ 0_{1 \times n} & 0_{1 \times n} & 0 & 0 & 0 \\ 0_{1 \times n} & 0_{1 \times n} & 0 & 0 & 0 \end{bmatrix}$$

$$\begin{pmatrix} \chi_{1} \\ \chi_{2} \\ \alpha \\ \dot{h} \end{pmatrix} + \begin{pmatrix} -B_{P}U\sin\alpha \\ B_{P}B_{v}(\chi; u) \\ 0 \\ 0 \\ 0 \end{pmatrix} + \begin{pmatrix} 0_{n \times 1} & 0_{n \times 1} \\ 0_{n \times 1} & 0_{n \times 1} \\ 0_{n \times 1} & 0_{n \times 1} \\ 0 \\ 0 \\ 0 \end{bmatrix} \begin{pmatrix} \ddot{\alpha} \\ \ddot{h} \end{pmatrix} \qquad (26)$$

where $B_{\rm v}(\chi; \boldsymbol{u})$ is given in Eq. (23) in terms of the states $\chi = [\chi_1, \chi_2, \alpha, \dot{\alpha}, \dot{h}]^T$ and the inputs $\boldsymbol{u} = [\ddot{\alpha}, \ddot{h}]^T$. The output equation for the total viscous unsteady loads is then written as

$$\begin{pmatrix}
L \\
M_{0}
\end{pmatrix}
= \left[U \mathbb{F} C_{P} \mathbb{F} C_{P} \ 0_{2\times 1} - U D_{P} b \left(\frac{1}{2} - a \right) \mathbb{F} + \mathbb{C}(1) \ U D_{P} \mathbb{F} \cos \alpha + \mathbb{C}(2) \right]$$

$$\begin{pmatrix}
\chi_{1} \\
\chi_{2} \\
\alpha \\
\dot{\alpha} \\
\dot{\alpha}
\end{pmatrix}
+ B_{v}(\chi; \boldsymbol{u}) \mathbb{F} t - U^{2} D_{P} \sin \alpha \mathbb{F} + \mathbb{M} \begin{pmatrix} \ddot{\alpha} \\ \ddot{h} \end{pmatrix} \tag{27}$$

where \mathbb{M} and \mathbb{C} are defined in Eq. (19), $\mathbb{C}(j)$ is the jth column of \mathbb{C} , and $\mathbb{F}' = D_p \mathbb{F} + \begin{pmatrix} 0 \\ \pi \rho b^2 \end{pmatrix}$.

B. Model Validation

To assess the accuracy of the developed model, computational fluid dynamic simulations of a pitching NACA 0012 airfoil are performed using ANSYS Fluent. The computational setup was developed and refined in our earlier efforts [57,82,83]; only its main features are described in the following. A hybrid mesh was constructed where the airfoil is enclosed by a fine structured grid that is linked to the far-field boundary through an unstructured triangular mesh zone. There are 300 nodes on each side of the airfoil and a total number of cells of about 200,000 in the entire domain. The mesh resolution is denser near the airfoil and wake, and it becomes coarser when approaching the far-field boundaries. This technique helps maintain a high-quality mesh resolution near the surface and can accommodate the airfoil motion through a dynamic mesh. The Reynolds number was set to $R = 10^5$, and the unsteady Reynolds-averaged Navier–Stokes (URANS) equations

were solved using the $k-\omega$ shear-stress transport turbulence model. Velocity inlet and pressure outlet boundary conditions were adopted at the far field, and the no-slip boundary condition was set at the airfoil surface. It was ensured that y^+ remains under one during all simulations. The inlet flow turbulent intensity was set to 0.1%, and the gauge pressure at the outlet boundary condition was set to zero. This computational setup was validated against experimental data in Refs. [82,83]. For more details of the simulation setup, boundary conditions, and dynamic mesh, the reader is referred to Refs. [57,82,83].

The state-space model presented in Eqs. (26) and (27) is simulated for the case of a pitching plate around the midchord point at $R = 10^5$ and k = 1. The following nonharmonic waveform is used to demonstrate the power of the developed state-space model in simulating arbitrary time-varying airfoil motion, in contrast to the frequency response model developed in our earlier effort [57]

$$\alpha(t) = A_{\alpha}(e^{\sin \omega t} - 1) \tag{28}$$

where A_{α} is set to ensure that the maximum α throughout the cycle is 1 deg. Figure 6 shows the lift and pitching moment (at the hinge point; i.e., quarter-chord) coefficients resulting from the state-space model [Eqs. (26) and (27)] in comparison to the potential-flow simulation (i.e., $B_v = 0$). Both results are compared in reference to the relatively higher-fidelity simulations of the URANS equations described earlier in this paper. In simulating the viscous statespace model [Eqs. (26) and (27)], the following potential-flow finite-state model is adopted, which is similar to that of Leishman and Beddoes [84]:

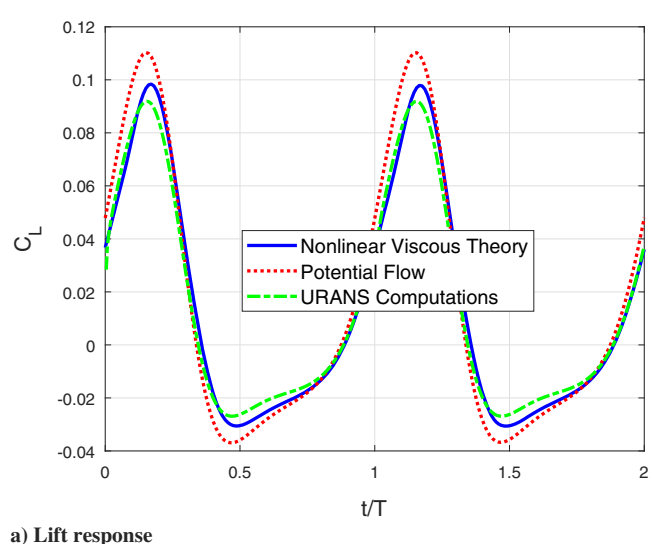
$$A_{P} = \frac{U}{b} \begin{bmatrix} -b_1 & 0 \\ 0 & -b_2 \end{bmatrix}, \qquad B_{p} = \frac{U}{b} \begin{pmatrix} b_1 A_1 \\ b_2 A_2 \end{pmatrix},$$

$$C_{P} = \begin{bmatrix} 1 & 1 \end{bmatrix}, \qquad D_{P} = 1 - A_1 - A_2$$

where the constants A_1 , A_2 , b_1 , and b_2 are those defining Jones's two-state approximation [14]

$$\phi(\tau) = 1 - A_1 e^{-b_1 \tau} - A_2 e^{-b_2 \tau}$$

of the Wagner function, where $\tau = (Ut/b)$. Their values are: $A_1 = 0.165$, $A_2 = 0.335$, $b_1 = 0.0445$, and $b_2 = 0.3$. In the Appendix, we show that this two-state approximation by Jones is one of the best approximations in the literature in terms of the tradeoff between accuracy and controllability/observability properties.



b) Pitching moment response

significant deviation from the classical potential-flow theory at this very small-amplitude oscillation (maximum α is 1 deg) but relatively large frequency (k = 1). It is also interesting to report a very good matching between the computational results and the developed statespace model. Indeed, it should serve aerodynamicists better than the classical Theodorsen model because it transcends the latter in the following aspects:

Inspecting the results shown in Fig. 6, it is interesting to observe

- 1) it provides viscous effects (i.e., Reynolds number dependence).
- 2) It captures nonlinearity and additional lag in the lift dynamics due to viscosity, which will affect instability boundaries.
- 3) It allows simulation of arbitrary time-varying airfoil motions (i.e., not confined to harmonic motions).
- 4) Being in a state-space form makes it much more convenient than a frequency response function for simulation and coupling with structural dynamics to perform aeroelasticity, flight dynamics analysis, and control design.
 - 5) It is simply more accurate.

IV. Linearization of the Nonlinear Viscous **Unsteady Theory**

Although the state-space model [Eqs. (26) and (27)] is indeed useful in simulation and analysis, it is always encouraging to seek analytical results. This goal is typically hard to achieve with a nonlinear theory, which invokes linearization of the nonlinear viscous unsteady theory developed earlier in this paper. Moreover, one drawback in the developed theory is its inability to tackle larger angles of attack; if α_e exceeds 0.47 (which corresponds to $\alpha \sim 3$ deg), the simulation must be terminated, which poses a good research problem on how to extend such a model (specifically, Fig. 2a) to at least relatively larger angles of attack below stall (up to $\alpha \sim 10$ deg), perhaps by matching a given steady $C_L - \alpha$ curve [21]. It should be noted that the classical inviscid theory (e.g., Theodorsen model) suffers from the same issue of validity over a small- α range. Yet, it does not stipulate terminating the simulation if the angle of attack exceeds a certain value. Therefore, insofar as the inability to continue simulation of the developed theory is a limiting factor, it is an advantage beyond the classical theory in the sense that it precisely defines a region of applicability. Having said that, this issue will be circumvented any way in the linearized model below, realizing that linearization is typically valid for sufficiently small disturbances.

A. Analytical Representation of the Viscous Lift Frequency Response

It is indeed intriguing to develop an analytical representation of the viscous unsteady lift frequency response, similar to the Theodorsen model, that depends not only on the frequency but also on the

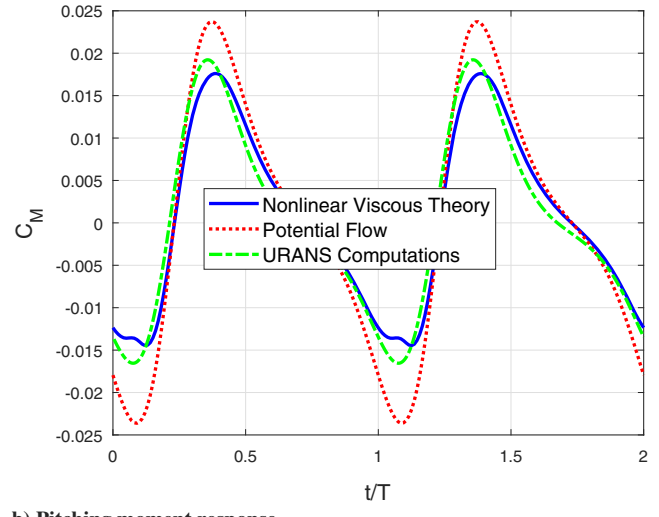


Fig. 6 Response of nonlinear state-space model [Eqs. (26) and (27)] of viscous lift and pitching moment (at hinge point; i.e., quarter-chord) to nonharmonic pitching maneuver [Eq. (28)] in comparison to potential-flow and URANS computations.

Reynolds number. This goal is pursued in the following by simply linearizing the nonlinear viscous unsteady theory developed earlier in this paper.

Equation (25) [or Eq. (14)] implies

$$L = L_P - 2\pi \rho b B_y$$

The potential-flow lift L_P only possesses geometric nonlinearities; hence, it can be easily linearized, resulting in the Theodrsen transfer function of the circulatory lift. Therefore, the main nonlinearity in the developed theory of the viscous unsteady lift resides in $B_{\rm v}$, which stems from the viscous triple-deck boundary-layer theory, as shown in the block diagram in Fig. 4. The $B_{\rm v}$ contribution possesses two nonlinearities: the nonlinearity of the relation $B_e(\alpha_e)$ shown in Fig. 2a, and a multiplicative nonlinearity represented by the term $\alpha_{\rm eff} \times B_e$ in Eq. (23). Expanding $B_{\rm v}$ in a Taylor series around the origin ($\chi=0$, u=0) and retaining only linear terms, we write

$$B_{v}(\boldsymbol{\chi};\boldsymbol{u}) \simeq B_{v}(0;0) - 2\epsilon^{3}\lambda^{-5/4}U^{2}[\alpha_{\text{eff}}(0;0)\Delta B_{e}(\alpha_{e}(0;0)) + B_{e}(\alpha_{e}(0;0))\Delta \alpha_{\text{off}}(0;0)]$$

where Δ represents first-order variations. Equation (22) implies that $\alpha_{\rm eff}(0;0)=0$, which results in zero α_s and α_e . This zero α_e , when plugged in the relation $B_e(\alpha_e)$ of Fig. 2a, results in $B_e(\alpha_e(0;0)) \triangleq B_{e_0} = 0.53$. Moreover, the first-order variation of B_e at zero is almost zero; $B_e(\alpha_e)$ has an almost-zero slope at $\alpha_e=0$. Hence, we have

$$B_{\rm v}(\boldsymbol{\chi};\boldsymbol{u}) \simeq -2\epsilon^3 \lambda^{-5/4} U^2 B_{e_0} \Delta \alpha_{\rm eff}(0;0)$$

Substituting the first variations of $\alpha_{\rm eff}$ from Eq. (21), we obtain the following linearization of $B_{\rm v}$

$$B_{v}(\chi; \mathbf{u}) \simeq -2\epsilon^{3} \lambda^{-5/4} B_{e_{0}} \left[U(\Delta v_{3/4}) C(k) - \frac{3}{2} b U \dot{\alpha} + 2b \Delta \dot{v}_{1/2} - b^{2} \ddot{\alpha} \right]$$
(29)

where

$$\Delta v_{3/4} = \dot{h} - b \left(\frac{1}{2} - a \right) \dot{\alpha} - U \alpha$$
, and $\Delta \dot{v}_{1/2} = \ddot{h} + ab \ddot{\alpha} - U \dot{\alpha}$ (30)

Recalling the classification of lift in Eq. (14) and interpreting the viscous contribution as circulatory (since it is associated with an additional circulation) (i.e., assuming the noncirculatory loads remain intact), the linearized viscous circulatory lift is then written as

$$L_{C} = -2\pi\rho b \times \left[Uv_{3/4} - 2\epsilon^{3}\lambda^{-5/4}B_{e_{0}} \left(Uv_{3/4}C(k) - \frac{3}{2}bU\dot{\alpha} + 2b\dot{v}_{1/2} - b^{2}\ddot{\alpha} \right) \right] C(k)$$
(31)

Unlike the inviscid theory, there is no special point (e.g., the three-quarter-chord point) over the airfoil whose angle of attack solely dictates the circulatory lift. The lift response depends on the motion in a complicated way; it would not be possible to obtain a lift transfer function independent of kinematics. Nevertheless, we can derive analytical representations of the lift transfer function for harmonic pitching and plunging separately. In both cases, we define the viscous lift frequency response function $C_{\rm v}$, similar to the Theodorsen model, as

$$C_{\rm v}(k;R) \triangleq \frac{L_C(k;R)}{L_{OS}(k)}$$

where L_{QS} is the quasi-steady lift given by $L_{QS} = -2\pi\rho bUv_{3/4}$.

1. Frequency Response due to Plunging

For a harmonic plunging motion $h(t) = He^{i\omega t}$, $v_{3/4} = \dot{h}$ and $\dot{v}_{1/2} = \ddot{h}$. As such, we obtain the viscous lift frequency response function

$$C_{\text{v,Plunging}}(k;R) = \left[1 - 2R^{-3/8}\lambda^{-5/4}B_{e_0}(C(k) + 2ik)\right]C(k)$$
 (32)

2. Frequency Response due to Pitching

For a harmonic pitching motion $\alpha(t) = A_{\alpha}e^{i\omega t}$,

$$v_{3/4} = -U\sin\alpha - \dot{\alpha}b\left(\frac{1}{2} - a\right)$$

and $\dot{v}_{1/2} = ab\ddot{\alpha} - U\cos\alpha\dot{\alpha}$, resulting in

$$\Delta v_{3/4}(k) = -UA_{\alpha} \left[1 + ik \left(\frac{1}{2} - a \right) \right], \quad \text{and}$$

$$\Delta \dot{v}_{1/2}(k) = -\frac{U^2}{h} A_a [ak^2 + ik]$$

As such, we obtain the viscous lift frequency response function

$$C_{\text{v,Pitching}}(k;R) = \left[1 - 2R^{-3/8}\lambda^{-5/4}B_{e_0}\left(C(k) + \frac{\frac{7}{2}ik - (1 - 2a)k^2}{1 + ik(1/2 - a)}\right)\right]C(k)$$
(33)

Equations (32) and (33) represent, for the first time, analytical representations of the viscous lift frequency response. That is, one can account for the Reynolds number dependence in an explicit way. Clearly, as $R \to \infty$, both transfer functions (of pitching and plunging) $C_v \to C(k)$; one recovers the inviscid behavior as the Reynolds number approaches infinity. Therefore, these two functions may replace the Theodorsen function in future analysis. Figure 7 shows the variations of these two viscous lift frequency response functions with reduced frequency at different Reynolds numbers in comparison to the inviscid response of the Theodorsen theory. Although the theory does not predict a considerable change in the magnitude of the transfer function from the inviscid response, it predicts a significant deviation in phase; the larger the frequency and the lower the Reynolds number, the larger the deviation in phase from the Theodorsen phase. These results were observed in our earlier effort [57] using a describing function analysis of the nonlinear theory. They are also captured here by the simple analytical relations [Eqs. (32) and (33)]. For a discussion about the physical reason behind this viscosity-induced lag and its relation to the Kutta condition, the reader is referred to our earlier effort [57].

The obtained phase results are also in accordance with the experimental results of Chu and Abramson [46], Henry [42], Abramson and Ransleben [64], and Bass et al. [39]. In these experimental efforts, the authors reconciled the deviation between the Theodorsen prediction of the unsteady aerodynamic loads and their measurements by adding some suggested phase lag to the Theodorsen function, which is naturally captured in the developed viscous theory. For example, Chu and Abramson [46] suggested adding a phase lag of -10 deg to the Theodorsen function for a better estimate of the unsteady lift and flutter boundary when $k \simeq 0.5$. Bass et al. [39] conducted a water-tunnel experiment for a NACA 16-012 undergoing pitching oscillations around its quarter-chord point in the ranges of 0.5 < k < 10 and R = 6500-26,500. They compared their force measurements to the Theodorsen potential-flow frequency response. They found bad agreement in the range of 0.5 < k < 2, where the most pronounced boundary-layer activity is observed and the flow near the trailing edge is separating and alternating around the trailing edge. They concluded that adding a phase lag of -30 deg to the Theodorsen C(k) would make the predicted lift from the classical theory of unsteady aerodynamics match their experimental measurements over this range. Similarly, there are several efforts in the

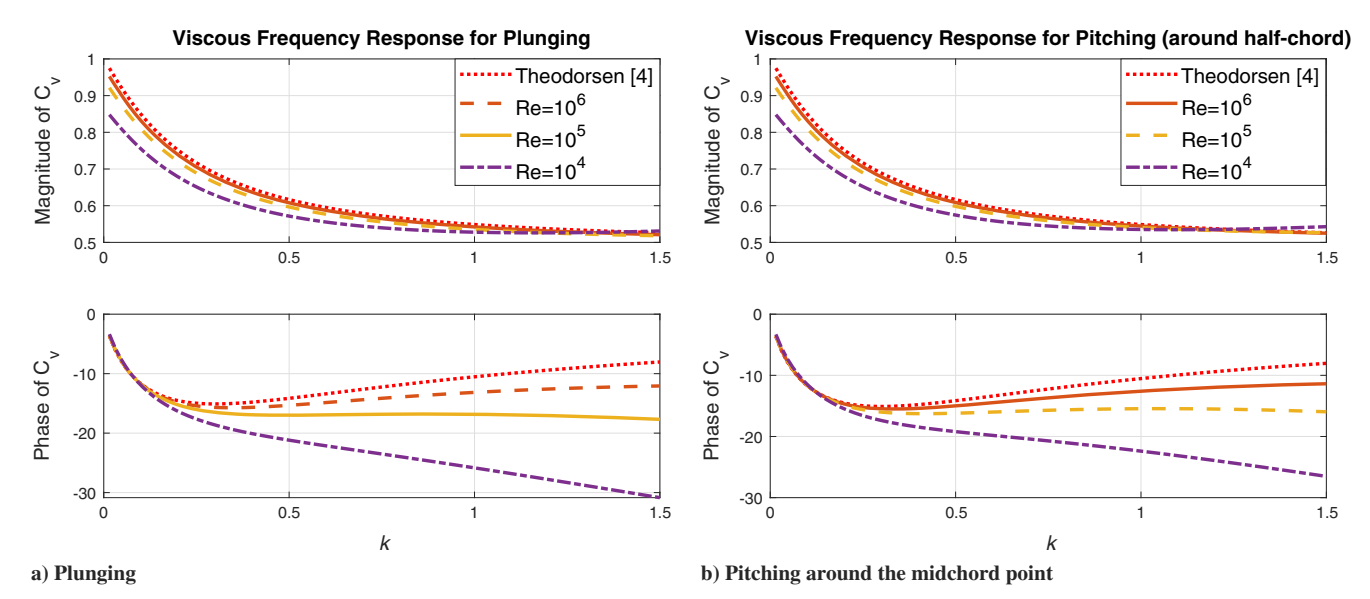


Fig. 7 Variation of viscous lift frequency response with Reynolds number in the case of plunging and pitching (around the midchord) in comparison to inviscid response of Theodorsen [4].

literature that suggest adding phase lag to the Theodorsen inviscid frequency response. However, there was no theoretical model that could predict the appropriate phase lag at a given combination of frequency and Reynolds number. The developed viscous unsteady theory fills this gap by providing a reasonable estimate of such a phase lag. This result is particularly important for flutter calculation. Note that the flutter instability, similar to any typical Hopf bifurcation, is mainly dictated by when energy is added/subtracted during the cycle. That is, the phase difference between the applied loads (aerodynamic loads) and the system motion (e.g., angle of attack) plays a crucial role in dictating the stability boundary. Therefore, if the Theodorsen model does not capture such a phase lag accurately, it may lead to a deviation in the flutter boundary. As such, it is expected that the developed viscous frequency response will result in a more accurate, yet efficient, estimate of the flutter boundary.

To present an example for the importance of the viscosity-induced phase lag and shift in the center of pressure for estimating the flutter boundary, we perform the standard *typical-section* flutter analysis [72,85] of the following wing:

$$m=0.2$$
 slug, $b=3$ ft, $I_{\alpha}=0.45$ slug · ft², $K_h=15.3$ lb/ft, $K_{\alpha}=98.5$ lb · ft/rad

where m is the mass of the wing, I_{α} is its pitching moment of inertia about the elastic axis, and K_h and K_{α} represent the bending and torsional stiffness of the wing section. Also, the elastic axis is located ab behind the midchord point, and the section center of mass is located $x_{\alpha}b$ behind the elastic axis with

$$x_a = -0.1$$
 and $a = 0.1$

Applying the standard typical-section flutter calculations [72,85] on this example using the Theodorsen inviscid lift dynamics and the proposed viscous lift dynamics, we obtain the following results for the flutter speed U_F and reduced frequency k_F :

$$k_F|_{\text{Theodorsen}} = 0.28$$
, $U_F|_{\text{Theodorsen}} = 123.6$ ft/s, $k_F|_{\text{Viscous}} = 0.40$ and $U_F|_{\text{Viscous}} = 87.4$ ft/s

That is, we observe more than 40% deviation in the flutter speed from the Theodorsen method and an even larger deviation in the flutter reduced frequency. To obtain this estimate, a Reynolds number of 10^6 is assumed whose associated Reynolds number based on turbulent viscosity is approximately 10^5 ; we used the latter value in our

viscous model. It should be noted that although the developed viscous unsteady model is validated in this paper, the corresponding flutter boundary remains to be validated using a high-fidelity fluid–structure-interaction computational or experimental model, which will be the focus of our future work.

Finally, it may be interesting to discuss the following point. Unlike the pitching case, where it is hard to interpret the $\dot{\alpha}$ terms in the viscous correction as circulatory or noncirculatory (since both contributions in potential flow include $\dot{\alpha}$ terms), such a classification is straightforward in the plunging case. In this case, the total viscous unsteady lift can be written as

$$L = \underbrace{\frac{-\pi\rho b^2\dot{v}_{1/2}}{\text{Noncirculatory}}}_{\text{Inviscid}} \underbrace{\frac{-2\pi\rho bUv_{3/4}C(k)}{\text{Circulatory}}}_{\text{Inviscid}} \\ -\underbrace{2R^{-3/8}\lambda^{-5/4}B_{e_0}(-2\pi\rho bUv_{3/4}C^2(k) - 4\pi\rho b^2\dot{v}_{1/2})}_{\text{Viscous}}$$

which suggests classifying the $v_{3/4}$ term in the viscous contribution as circulatory and the $\dot{v}_{1/2}$ term as noncirculatory (added mass). By doing so, we obtain a viscous frequency response of the circulatory lift as

$$C_{v}(k;R) = [1 - 2R^{-3/8}\lambda^{-5/4}B_{e_0}C(k)]C(k)$$

simultaneously with a viscous (i.e., Reynolds-number-dependent) added mass that is also frequency dependent:

$$m_{\rm v}(k;R) = \pi \rho b^2 \left[1 - 8R^{-3/8} \lambda^{-5/4} B_{e_0} C(k) \right]$$
 (34)

Following this classification, the resulting viscous frequency response C_v of the circulatory lift is quite close to the Theodorsen method. That is, the main viscous contribution actually resides in the acceleration term, which explains why the viscous response deviates from the Theodorsen response at higher frequencies. Therefore, this discussion suggests that, for pure plunging, one can model the viscous effects by just considering the modified (decreased) frequency-dependent added mass m_v given in Eq. (34).

B. Analytical Linear State-Space Representation of Viscous Unsteady Loads

Since the nonlinear state-space model [Eqs. (26) and (27)] is valid only for small angles, it may be prudent to develop a linearized version of it. Having linearized the viscous frequency response

theory (developed earlier [57]) to obtain the analytical frequency response functions [Eqs. (32) and (33)], it should be straightforward to linearize the nonlinear state-space model [Eqs. (26) and (27)]. The geometric nonlinearities in the model [Eqs. (26) and (27)] can be easily linearized; the main nontrivial nonlinear term is B_v , which has been already linearized earlier in this paper, as given in Eq. (29) in the frequency domain. Therefore, it can be written in the time domain as

$$B_{v}(\boldsymbol{\chi};\boldsymbol{u}) \simeq -2\epsilon^{3}\lambda^{-5/4}B_{e_{0}}\left[Uy_{P} - \frac{7}{2}bU\dot{\alpha} + 2b\ddot{h} - (1-2a)b^{2}\ddot{\alpha}\right]$$

where y_P is the output from the potential-flow state-space model [Eq. (16)], i.e., the time-domain version of $v_{3/4}C(k)$. Substituting y_P from Eq. (16) and the linearized $v_{3/4}$ from Eq. (30), then B_v can be written linearly in the states in the time domain as

$$B_{v}(\boldsymbol{\chi};\boldsymbol{u}) \simeq -R_{L} \left[U(\boldsymbol{C}_{P}\boldsymbol{\chi}_{1} + D_{P}\boldsymbol{H}_{3/4}\boldsymbol{\chi}_{3}) - \frac{7}{2}bU\dot{\alpha} + 2b\ddot{h} - (1 - 2a)b^{2}\ddot{\alpha} \right]$$
(35)

where $R_L = 2R^{-3/8}\lambda^{-5/4}B_{e_0}$ is a constant (related to the effect of the Reynolds number R on lift), χ_3 is the third set of states $\chi_3 = [\alpha, \dot{\alpha}, \dot{h}]^T$, and $H_{3/4}$ defines the linear dependence of $v_{3/4}$ on χ_3 :

$$\Delta v_{3/4} = \begin{bmatrix} -U & -b(\frac{1}{2} - a) & 1 \end{bmatrix} \begin{pmatrix} \alpha \\ \dot{\alpha} \\ \dot{b} \end{pmatrix} \triangleq H_{3/4} \chi_3 \qquad (36)$$

As such, the nonlinear state-space model [Eqs. (26) and (27)] can then be linearized into the following form:

$$\frac{d}{dt} \begin{pmatrix} \chi_{1} \\ \chi_{2} \\ \chi_{3} \end{pmatrix} = \begin{bmatrix} A_{P} & 0_{n \times n} & B_{P} H_{3/4} \\ -UR_{L} B_{P} C_{P} & A_{P} & -UR_{L} D_{P} B_{P} H_{3/4} \\ 0_{3 \times n} & 0_{3 \times n} & 0_{3 \times 3} \end{bmatrix} \begin{pmatrix} \chi_{1} \\ \chi_{2} \\ \chi_{3} \end{pmatrix} + \begin{bmatrix} 0_{n \times 1} & 0_{n \times 1} & 0_{n \times 1} \\ \frac{7}{2} UbR_{L} B_{P} & (1 - 2a)b^{2} R_{L} B_{P} & -2bR_{L} B_{P} \\ I_{3 \times 3} \end{bmatrix} \begin{pmatrix} \dot{\alpha} \\ \ddot{\alpha} \\ \ddot{n} \end{pmatrix} (37)$$

and the output equation can be written in the linear form:

a) Lift response

$$\begin{pmatrix}
L \\
M_0
\end{pmatrix} = \left[U(\mathbb{F} - R_L D_p \mathbb{F}') C_P \quad \mathbb{F} C_P \quad U D_P (\mathbb{F} - R_L D_p \mathbb{F}') H_{3/4} \right] \\
\begin{pmatrix}
\chi_1 \\
\chi_2 \\
\gamma_\nu
\end{pmatrix} - \frac{\pi}{2} \rho U b^2 \begin{pmatrix}
-2(1 - 7R_L D_p) \\
b[1 - 7R_L (1 - D_p)]
\end{pmatrix} \dot{\alpha} + \mathbb{M}_v \begin{pmatrix} \ddot{\alpha} \\ \ddot{h} \end{pmatrix} \quad (38)$$

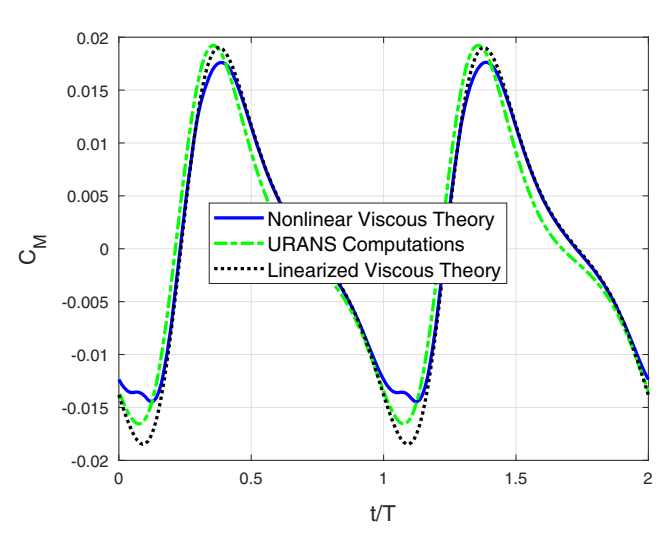
where \mathbb{M}_{v} represents the viscous version of the mass matrix \mathbb{M} and is given by

$$\mathbb{M}_{v} = -\pi \rho b^{2} \begin{bmatrix} b[a + 2R_{L}D_{p}(1 - 2a)] & 1 - 4R_{L}D_{p} \\ b^{2} \left[\frac{1}{8} - R_{L}(1 - 2a)(1 - D_{p}) \right] & 2R_{L}b(1 - D_{p}) \end{bmatrix}$$
(39)

Figure 8 shows the simulation of the linearized viscous state-space model [Eqs. (37) and (38)] subject to the nonharmonic small-amplitude maneuver defined in Eq. (28). As expected, for small-amplitude maneuvers such as the one considered here, the response of the linearized viscous system matches that of the nonlinear system [Eqs. (26) and (27)] well; both match the higher-fidelity URANS simulations. As such, the simple four-state (plus three kinematic states) system [Eqs. (37) and (38)] is expected to be of a significant benefit to aeroelasticians and flight dynamic-ists because it captures viscous unsteady effects in a convenient dynamical-system form (state-space form), allowing efficient simulation and coupling with structural dynamics for linear stability analysis (e.g., flutter analysis) and control design.

V. Conclusions

In this paper, a nonlinear state-space model of viscous unsteady aerodynamic loads was developed. The model presents a finite-state approximation of the recently developed infinite-dimensional viscous, unsteady aerodynamic theory that couples potential flow with the tripledeck boundary-layer theory. The model uses the Wiener-Hammerstein structure and consists of four internal aerodynamic states and three kinematic states. It is validated against relatively higher-fidelity computations of the unsteady Reynolds-averaged Navier-Stokes equations. Comparisons show that the potential-flow results could deviate significantly from the viscous theory, even for a very small-amplitude oscillation (down to 1 deg1°) when the reduced frequency is relatively large. Moreover, the developed nonlinear state-space model is in very good agreement with the URANS predictions of the lift and moment over a specified range of angle of attack. Therefore, this model will be of paramount importance to aeroelasticians and flight dynamicists because 1) it captures viscous Reynolds number effects, including nonlinearity



b) Pitching moment response

Fig. 8 Response of linear state-space model [Eqs. (37) and (38)] of viscous lift and pitching moment (at hinge point; i.e., quarter-chord) to nonharmonic pitching maneuver [Eq. (28)] in comparison to nonlinear model [Eqs. (26) and (27)] and URANS computations.

and additional lag in the lift dynamics; 2) it allows simulation of arbitrary time-varying maneuvers (not necessarily harmonic); and 3) being in a state-space form, it allows straightforward coupling with structural dynamics for aeroelasticity and flight dynamics analysis and control design. Moreover, linearizing such a theory, a linear state-space model and an analytical representation of the viscous lift frequency response function were derived, which are explicit functions of both frequency and the Reynolds number.

Appendix: Finite-State Approximations of the Potential-Flow Lift Dynamics

There have been several finite-dimensional approximations of the potential-flow lift dynamics [13–19,22,23]. Since the viscous unsteady model (developed in this paper) includes potential-flow lift as a submodel, it may be prudent to present a comparison among the common finite-dimensional approximations of the infinite-dimensional potential-flow lift response, as well as to study whether a better approximation can be developed. In particular, we consider the behavior of the common finite-state approximations of Jones [14] and Vepa [16] in comparison to the MATLAB system identification algorithm *tfest*.

Jones [14] introduced the following two-state approximation of the Wagner function in the time domain

$$\phi(\tau) = 1 - A_1 e^{-b_1 \tau} - A_2 e^{-b_2 \tau} \tag{A1}$$

where $\tau = (Ut/b)$ is the nondimensional time; and

$$A_1 = 0.165$$
, $A_2 = 0.335$, $b_1 = 0.0445$, and $b_2 = 0.3$

It is one of the most common approximations in the literature. Taking the Laplace transform of the step response $\phi(\tau)$ and dividing it by the Laplace transform 1/s of the step input, we can easily write the corresponding transfer function

$$G_J(s) = \frac{(1 - A_1 - A_2)s^2 + (b_1 + b_2 - A_1b_2 - A_2b_1)s + b_1b_2}{s^2 + (b_1 + b_2)s + b_1b_2}$$
(A2)

Vepa [14] used the method of Padé approximants to develop a finite-dimensional approximation of the Theodorsen function in the frequency domain. His first four Padé approximants are given by

$$G_{V,1}(s) = \frac{s+0.5}{2s+0.5}, \qquad G_{V,2}(s) = \frac{s^2+1.5s+0.375}{2\ s^2+2.5s+0.375},$$

$$G_{V,3}(s) = \frac{s^3+3.5\ s^2+2.7125s+0.46875}{2\ s^3+6.5\ s^2+4.25s+0.46875}, \text{ and}$$

$$G_{V,4}(s) = \frac{s^4+4.64696s^3+9.33371\ s^2+5.51735s+0.49334}{2s^4+8.79392s^3+16.71894s^2+7.67296s+0.49334}$$
(A3)

He also used a least-squares (LS) approach to develop the following fourth 4th-order approximation of the potential-flow lift dynamics:

$$G_{V,LS}(s) = \frac{s^4 + 0.761036s^3 + 0.102058s^2 + 0.00255067s + 9.55732 \times 10^{-6}}{2s^4 + 1.063939s^3 + 0.113938s^2 + 0.0026168s + 9.55732 \times 10^{-6}}$$
(A4)

It is clear that, in all of these approximations, the high-frequency gain

$$\lim_{s\to\infty} G(s)$$

is 1/2 and the dc gain

$$\lim_{s\to 0} G(s)$$

is one [74]. The former implies the same order of the numerator and denominator of the transfer function; this fact was also necessary for Vepa [16] to structure the approximants. Using the same number of poles and zeros, one can use the MATLAB system identification algorithm *tfest* to develop a dynamical system from the frequency response data given by the Theodorsen function. The following fourth 4th-order system is obtained:

$$G_M(s) = \frac{0.5001s^4 + 0.8309s^3 + 0.356s^2 + 0.03972s + 0.0007756}{s^4 + 1.413s^3 + 0.47816s^2 + 0.04377s + 0007795}$$

(A5)

Note that this technique, being data driven, will depend on the range of frequencies considered in the estimation and its resolution. However, nice convergence is observed for large enough k range and fine enough resolution; the preceding transfer function was developed using a k range of 0–10 with 10,000 equidistant points.

Figure A1 shows the frequency response of Jones's [15] second 2nd-order transfer function [Eq. (A2)], Vepa's [16] second 2nd- and fourth 4th-order Padé approximants given in Eq. (A3), Vepa's fourth 4th-order LS transfer function [Eq. (A4)], and the fourth 4th-order transfer function [Eq. (A5)] identified using MATLAB'S *tfest* in comparison to the Theodorsen exact formula

$$C(k) = \frac{H_1^{(2)}(k)}{H_1^{(2)}(k) + iH_0^{(2)}(k)}$$

where $H_n^{(m)}$ is the Hankel function of the mth mth kind of order n. The figure shows that Vepa's Padé approximants experience some deviation from the exact response, whereas Vepa's fourth 4th-order LS and MATLAB'S fourth 4th-order transfer function are close to the Theodorsen exact response. Interestingly, Jones's transfer function [15], although only second 2nd order, captures the lift frequency response well (even better than Vepa's fourth 4th-order Padé approximant [16]).

It should be noted that accuracy is not the only goal when developing these finite-dimensional approximations. Since these approximations are mainly developed for dynamics and control analysis, it may be judicious to investigate their controllability and observability properties; an accurate approximation may be weakly controllable (or observable), and hence not so useful in control design (or estimation). To study the controllability and observability properties simultaneously, it is convenient to transform a given system into a balanced canonical form where the controllability and observability gramians are equal: $W_c = W_o$ [A1,A2]. Given a minimal realization (A, B, C, D) of any of the aforementioned approximate transfer functions [Eqs. (A2)–(A5)], the controllability and observability gramians are computed by solving the Lyapunov equations

$$AW_c + W_c A^T + BB^T = 0$$
 and $A^T W_o + W_o A + C^T C = 0$ (A6)

We then perform Cholesky factorization for W_c and W_o as

$$W_c = L_c L_c^T$$
 and $W_o = L_o L_o^T$

Finally, the controllability and observability gramians in the balanced form are equal and given by Σ , which comes from the singular value decomposition of $L_o^T L_c$; i.e., we have $L_o^T L_c = U \Sigma V^T$. We then consider the condition number of Σ as an indicator of how close it is to being singular (i.e., how weakly controllable the system is); the larger the condition number of Σ , the closer it is to being singular, indicating weaker controllability of the system.

Table A1 shows a comparison among the finite-dimensional approximations, presented earlier in this paper, of the potential-flow lift dynamics in terms of accuracy and controllability/observability properties; the former is represented by the root-mean-square (RMS) error/deviation from the Theodorsen exact response, and the latter is represented by the condition number of the controllability/observability gramian Σ in the balanced form. The table data corroborate the

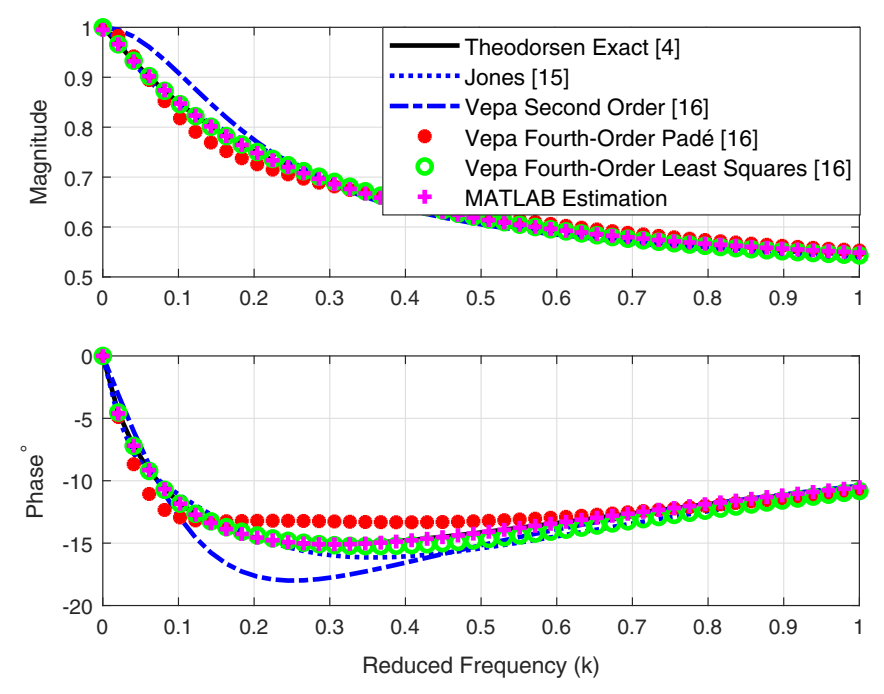


Fig. A1 Frequency response of different finite-dimensional approximations of the potential-flow lift.

Table A1 Comparison among different finite-dimensional approximations of potential-flow lift dynamics in terms of accuracy and controllability/observability properties

Author	Transfer function	RMS error, %	Condition number of Σ
Jones [14]	$\frac{0.5s^2 + 0.2808s + 0.0136}{s^2 + 0.3455s + 0.0136}$	1.28	6.17
Vepa second-2nd order Padé [16]	$\frac{s^2 + 1.5s + 0.375}{2s^2 + 2.5s + 0.375}$	2.93	22.96
Vepa fourth 4th-order Padé [16]	$\frac{s^4 + 4.64696s^3 + 9.33371s^2 + 5.51735s + 0.49334}{2s^4 + 8.79392s^3 + 16.71894s^2 + 7.67296s + 0.49334}$	1.83	1137.4
Vepa fourth 4th-order LS [16]	$\frac{s^4 + 0.761036s^3 + 0.102058s^2 + 0.00255067s + 9.55732 \times 10^{-6}}{2s^4 + 1.063939s^3 + 0.113938s^2 + 0.0026168s + 9.55732 \times 10^{-6}}$	0.55	147.42
MATLAB tfest fourth 4th order	$\frac{0.5001s^4 + 0.8309s^3 + 0.356s^2 + 0.03972s + 0.0007756}{s^4 + 1.413s^3 + 0.47816s^2 + 0.04377s + 0007795}$	0.08	140.74

behavior shown in Fig. A1: Vepa's Padé approximants [16] experience the largest error/deviation, relatively, although their absolute RMS may be satisfactory (RMS is less than 3%). It also shows that the MATLAB tfest identified fourth 4th-order model and Vepa's fourth 4th-order LS model are quite close to the exact response (RMSs are less than 0.1 and 1%, respectively). However, these accurate models are weakly controllable (due to a pole-zero pair close to cancelation). Interestingly, Vepa's fourth 4th-order Padé approximant suffers from the weakest controllability/observability, even though it does not enjoy a very high accuracy, excluding its candidacy as a good finite-state approximation of the potential-flow lift dynamics. Surprisingly, Jones's model (the first model developed in the literature [15]) enjoys the strongest controllability/observability properties along with a satisfactory accuracy (RMS is 1.28%) with even a low order, making it the best candidate among the selected group; the model that was developed in the 1940s without any consideration for controllability/observability (these concepts were developed later in the 1960s by Kalman et al. [A3]) turns out to be the most controllable/ observable approximation with a low order and high accuracy.

Acknowledgments

The authors would like to acknowledge the support of the National Science Foundation through grant CBET-2005541. The authors are also grateful to the computational efforts of Nabil Khalifa.

References

- [1] Prandtl, L., "Über die Entstehung von Wirbeln in der Idealen Flüssigkeit, mit Anwendung auf die Tragflügeltheorie und Andere Aufgaben," Vorträge aus dem Gebiete der Hydro- und Aerodynamik (Innsbruck 1922), Springer, New York, 1924, pp. 18–33.
- [2] Birnbaum, W., "Der Schlagflugelpropeller und die Kleinen Schwingungen Elastisch Befestigter Tragfluegel," Zeitschrift für Flugtech und Motorluftschiffahrt, Vol. 15, 1924, pp. 128–134.
- [3] Wagner, H., "Uber die Entstehung des Dynamischen Auftriebs von Tragflugeln," Zeitschrift für Angewandte Mathematik und Mechanik, Vol. 5, No. 1, 1925, pp. 17–35. https://doi.org/10.1002/zamm.19250050103
- [4] Theodorsen, T., "General Theory of Aerodynamic Instability and the Mechanism of Flutter," NACA TR 496, 1935.
- [5] von Kármán, T., and Sears, W. R., "Airfoil Theory for Non-Uniform Motion," *Journal of the Aeronautical Sciences*, Vol. 5, No. 10, 1938, pp. 379–390. https://doi.org/10.2514/8.674
- [6] Ansari, S. A., Żbikowski, R., and Knowles, K., "Non-Linear Unsteady Aerodynamic Model for Insect-Like Flapping Wings in the Hover. Part 1: Methodology and Analysis," *Journal of Aerospace Engineering*, Vol. 220, No. 2, 2006, pp. 61–83. https://doi.org/10.1243/09544100JAERO49
- [7] Tchieu, A. A., and Leonard, A., "A Discrete-Vortex Model for the Arbitrary Motion of a Thin Airfoil with Fluidic Control," *Journal of Fluids and Structures*, Vol. 27, No. 5, 2011, pp. 680–693. https://doi.org/10.1016/j.jfluidstructs.2011.02.008
- [8] Küssner, H. G., "Schwingungen von Flugzeugflügeln," Jahrbuch der Deutscher Versuchsanstalt für Luftfahrt, 1929, pp. 319–320.

[9] Schwarz, L., "Brechnung der Druckverteilung Einer Harmonisch sich Verformenden Tragflache in Ebener Stromung," Vol. 17, Luftfahrtforsch, Dec. 1940, pp. 379–386.

- [10] Sears, W. R., "Some Aspects of Non-Stationary Airfoil Theory and its Practical Application," *Journal of the Aeronautical Sciences*, Vol. 8, No. 3, 1941, pp. 104–108. https://doi.org/10.2514/8.10655
- [11] Loewy, R. G., "A Two-Dimensional Approximation to Unsteady Aerodynamics in Rotary Wings," *Journal of Aeronautical Sciences*, Vol. 24, No. 2, 1957, pp. 81–92. https://doi.org/10.2514/8.3777
- [12] Garrick, I. E., "On Some Reciprocal Relations in the Theory of Nonstationary Flows," NACA TR 629, 1938.
- [13] Peters, D. A., "Two-Dimensional Incompressible Unsteady Airfoil Theory—An Overview," *Journal of Fluids and Structures*, Vol. 24, No. 3, 2008, pp. 295–312. https://doi.org/10.1016/j.jfluidstructs.2007.09.001
- [14] Jones, R. T., "Operational Treatment of the Nonuniform Lift Theory to Airplane Dynamics," NACATR 667, 1938.
- [15] Jones, W. P., "Aerodynamic Forces on Wings in Non-Uniform Motion," British Aeronautical Research Council TR 2117, 1945.
- [16] Vepa, R., "On the Use of Padé Approximants to Represent Unsteady Aerodynamic Loads for Arbitrarily Small Motions of Wings," AIAA Paper 1976-17, 1976.
- [17] Leishman, J. G., and Nguyen, K. Q., "State-Space Representation of Unsteady Airfoil Behavior," *AIAA Journal*, Vol. 28, No. 5, 1990, pp. 836–844. https://doi.org/10.2514/3.25127
- [18] Peters, D. A., and Karunamoorthy, S., "State-Space Inflow Models for Rotor Aeroelasticity," AIAA Paper 1994-1920, 1994.
- [19] Peters, D. A., Karunamoorthy, S., and Cao, W., "Finite State Induced Flow Models, Part I: Two-Dimensional Thin Airfoil," *Journal of Aircraft*, Vol. 32, No. 2, March 1995, pp. 313–322.
 [20] Brunton, S. L., and Rowley, C. W., "Empirical State-Space Representa-
- [20] Brunton, S. L., and Rowley, C. W., "Empirical State-Space Representations for Theodorsen's Lift Model," *Journal of Fluids and Structures*, Vol. 38, 2013, pp. 174–186. https://doi.org/10.1016/j.jfluidstructs.2012.10.005
- [21] Taha, H., Hajj, M. R., and Beran, P. S., "State Space Representation of the Unsteady Aerodynamics of Flapping Flight," *Aerospace Science* and Technology, Vol. 34, 2014, pp. 1–11. https://doi.org/10.1016/j.ast.2014.01.011
- [22] Zakaria, M. Y., Taha, H., and Hajj, M. R., "Measurement and Modeling of Lift Enhancement on Plunging Airfoils: A Frequency Response Approach," *Journal of Fluids and Structures*, Vol. 69, 2017, pp. 187–208. https://doi.org/10.1016/j.jfluidstructs.2016.12.004
- [23] dos Santos, C. R., Pacheco, D. R. Q., Taha, H. E., and Zakaria, M. Y., "Nonlinear Modeling of Electro-Aeroelastic Dynamics of Composite Beams with Piezoelectric Coupling," *Composite Structures*, Vol. 255, 2020, Paper 112968.
- [24] Jones, M. A., "The Separated Flow of an Inviscid Fluid Around a Moving Flat Plate," *Journal of Fluid Mechanics*, Vol. 496, 2003, pp. 405–441. https://doi.org/10.1017/S0022112003006645
- [25] Yongliang, Y., Binggang, T., and Huiyang, M., "An Analytic Approach to Theoretical Modeling of Highly Unsteady Viscous Flow Excited by Wing Flapping in Small Insects," *Acta Mechanica Sinica*, Vol. 19, No. 6, 2003, pp. 508–516. https://doi.org/10.1007/BF02484543
- [26] Pullin, D. I., and Wang, Z., "Unsteady Forces on an Accelerating Plate and Application to Hovering Insect Flight," *Journal of Fluid Mechanics*, Vol. 509, 2004, pp. 1–21. https://doi.org/10.1017/S0022112004008821
- [27] Michelin, S., and Smith, S. G. L., "An Unsteady Point Vortex Method for Coupled Fluid–Solid Problems," *Theoretical and Computational Fluid Dynamics*, Vol. 23, No. 2, 2009, pp. 127–153. https://doi.org/10.1007/s00162-009-0096-7
- [28] Wang, C., and Eldredge, J. D., "Low-Order Phenomenological Modeling of Leading-Edge Vortex Formation," *Theoretical and Computational Fluid Dynamics*, Vol. 27, No. 5, 2013, pp. 577–598. https://doi.org/10.1007/s00162-012-0279-5
- [29] Ramesh, K., Gopalarathnam, A., Edwards, J. R., Ol, M. V., and Granlund, K., "An Unsteady Airfoil Theory Applied to Pitching Motions Validated Against Experiment and Computation," *Theoreti*cal and Computational Fluid Dynamics, Vol. 27, No. 6, 2013, pp. 843–864.
- [30] Ramesh, K., Gopalarathnam, A., Granlund, K., Ol, M. V., and Edwards, J. R., "Discrete-Vortex Method with Novel Shedding Criterion For Unsteady Aerofoil Flows with Intermittent Leading-Edge Vortex Shedding," *Journal of Fluid Mechanics*, Vol. 751, 2014, pp. 500–538. https://doi.org/10.1017/jfm.2014.297

- [31] Yan, Z., Taha, H., and Hajj, M. R., "Geometrically-Exact Unsteady Model for Airfoils Undergoing Large Amplitude Maneuvers," *Aerospace Science and Technology*, Vol. 39, 2014, pp. 293–306. https://doi.org/10.1016/j.ast.2014.09.021
- [32] Li, J., and Wu, Z.-N., "Unsteady Lift for the Wagner Problem in the Presence of Additional Leading/Trailing Edge Vortices," *Journal of Fluid Mechanics*, Vol. 769, 2015, pp. 182–217. https://doi.org/10.1017/jfm.2015.118
- [33] Hussein, A. A., Taha, H., Ragab, S., and Hajj, M. R., "A Variational Approach for the Dynamics of Unsteady Point Vortices," *Aerospace Science and Technology*, Vol. 78, 2018, pp. 559–568. https://doi.org/10.1016/j.ast.2018.05.010
- [34] Crighton, D. G., "The Kutta Condition in Unsteady Flow," Annual Review of Fluid Mechanics, Vol. 17, No. 1, 1985, pp. 411–445. https://doi.org/10.1146/annurev.fl.17.010185.002211
- [35] Howarth, L., "The Theoretical Determination of the Lift Coefficient for a Thin Elliptic Cylinder," *Proceedings of the Royal Society of London, Series A: Mathematical and Physical Sciences*, Vol. 149, No. 868, 1935, pp. 558–586.
- [36] Basu, B. C., and Hancock, G. J., "The Unsteady Motion of a Two-Dimensional Aerofoil in Incompressible Inviscid Flow," *Journal of Fluid Mechanics*, Vol. 87, No. 1, 1978, pp. 159–178. https://doi.org/10.1017/S0022112078002980
- [37] Daniels, P. G., "On the Unsteady Kutta Condition," *Quarterly Journal of Mechanics and Applied Mathematics*, Vol. 31, No. 1, 1978, pp. 49–75. https://doi.org/10.1093/qjmam/31.1.49
- [38] Satyanarayana, B., and Davis, S., "Experimental Studies of Unsteady Trailing-Edge Conditions," AIAA Journal, Vol. 16, No. 2, 1978, pp. 125–129. https://doi.org/10.2514/3.60869
- [39] Bass, R. L., Johnson, J. E., and Unruh, J. F., "Correlation of Lift and Boundary-Layer Activity on an Oscillating Lifting Surface," AIAA Journal, Vol. 20, No. 8, 1982, pp. 1051–1056. https://doi.org/10.2514/3.7964
- [40] Rott, N., and George, M. B. T., "An Approach to the Flutter Problem in Real Fluids," Inst. of the Aeronautical Sciences, TR 509, 1955.
- [41] Abramson, H. N., and Chu, H.-H., "A Discussion of the Flutter of Submerged Hydrofoils," *Journal of Ship Research*, Vol. 3, No. 2, 1959, pp. 5–13.
- [42] Henry, C. J., "Hydrofoil Flutter Phenomenon and Airfoil Flutter Theory," Davidson Lab. TR 856, New Jersey, 1961.
- [43] Chu, W.-H., "An Aerodynamic Analysis for Flutter in Oseen-Type Viscous Flow," *Journal of the Aerospace Sciences*, Vol. 29, No. 7, 1962, pp. 781–789. https://doi.org/10.2514/8.9606
- [44] Shen, S. F., and Crimi, P., "The Theory for an Oscillating Thin Airfoil as Derived from the Oseen Equations," *Journal of Fluid Mechanics*, Vol. 23, No. 3, 1965, pp. 585–609. https://doi.org/10.1017/S0022112065001568
- [45] Woolston, D. S., and Castile, G. E., "Some Effects of Variations in Several Parameters Including Fluid Density on TBE Flutter Speed of Light Uniform Cantilever Wings," NACATR 2558, 1951.
- [46] Chu, W.-H., and Abramson, H. N., "An Alternative Formulation of the Problem of Flutter in Real Fluids," *Journal of the Aerospace Sciences*, Vol. 26, No. 10, 1959, pp. 683–684. https://doi.org/10.2514/8.8259
- [47] Abramson, H. N., Chu, W.-H., and Irick, J. T., "Hydroelasticity with Special Reference to Hydrofoil Craft," Naval Ship Research and Development Center, Hydromechanics Lab. TR 2557, 1967.
- [48] Savage, S. B., Newman, B. G., and Wong, D. T.-M., "The Role of Vortices and Unsteady Effects during the Hovering Flight of Dragonflies," *Journal of Experimental Biology*, Vol. 83, No. 1, 1979, pp. 59–77. https://doi.org/10.1242/jeb.83.1.59
- [49] Orszag, S. A., and Crow, S. C., "Instability of a Vortex Sheet Leaving a Semi-Infinite Plate," *Studies in Applied Mathematics*, Vol. 49, No. 2, 1970, pp. 167–181. https://doi.org/10.1002/sapm1970492167
- [50] Ansari, S. A., Zbikowski, R., and Knowles, K., "Non-linear Unsteady Aerodynamic Model for Insect-Like Flapping Wings in the Hover. Part 2: Implementation and Validation," *Journal of Aerospace Engineering*, Vol. 220, No. 3, 2006, pp. 169–186.
- [51] Pitt Ford, C. W., and Babinsky, H., "Lift and the Leading-Edge Vortex," Journal of Fluid Mechanics, Vol. 720, 2013, pp. 280–313. https://doi.org/10.1017/jfm.2013.28
- [52] Hemati, M. S., Eldredge, J. D., and Speyer, J. L., "Improving Vortex Models via Optimal Control Theory," *Journal of Fluids and Structures*, Vol. 49, 2014, pp. 91–111. https://doi.org/10.1016/j.jfluidstructs.2014.04.004
- [53] Zakaria, M. Y., Taha, H. E., and Hajj, M. R., "Design Optimization of Flapping Ornithopters: The Pterosaur Replica in Forward Flight,"

- Journal of Aircraft, Vol. 53, No. 1, 2016, pp. 48–59. https://doi.org/10.2514/1.C033154
- [54] Hussein, A. A., Seleit, A. E., Taha, H. E., and Hajj, M. R., "Optimal Transition of Flapping Wing Micro-Air Vehicles from Hovering to Forward Flight," *Aerospace Science and Technology*, Vol. 90, 2019, pp. 246–263. https://doi.org/10.1016/j.ast.2019.04.043
- [55] Al-Haik, M. Y., Zakaria, M. Y., Hajj, M. R., and Haik, Y., "Storage of Energy Harvested from a Miniature Turbine in a Novel Organic Capacitor," *Journal of Energy Storage*, Vol. 6, 2016, pp. 232–238. https://doi.org/10.1016/j.est.2016.01.008
- [56] Xia, X., and Mohseni, K., "Unsteady Aerodynamics and Vortex-Sheet Formation of a Two-Dimensional Airfoil," *Journal of Fluid Mechanics*, Vol. 830, 2017, pp. 439–478. https://doi.org/10.1017/jfm.2017.513
- [57] Taha, H., and Rezaei, A. S., "Viscous Extension of Potential-Flow Unsteady Aerodynamics: The Lift Frequency Response Problem," *Journal of Fluid Mechanics*, Vol. 868, 2019, pp. 141–175. https://doi.org/10.1017/jfm.2019.159
- [58] Zhu, W., McCrink, M. H., Bons, J. P., and Gregory, J. W., "The Unsteady Kutta Condition on an Airfoil in a Surging Flow," *Journal of Fluid Mechanics*, Vol. 893, 2020. https://doi.org/10.1017/jfm.2020.254
- [59] Stewartson, K., "On the Flow near the Trailing Edge of a Flat Plate," Proceedings of the Royal Society of London, Series A: Mathematical, Physical and Engineering Sciences, Vol. 306, No. 1486, 1968, pp. 275–290.
- [60] Messiter, A. F., "Boundary-Layer Flow near the Trailing Edge of a Flat Plate," SIAM Journal on Applied Mathematics, Vol. 18, No. 1, 1970, pp. 241–257. https://doi.org/10.1137/0118020
- [61] Brown, S. N., and Stewartson, K., "Trailing-edge stall," *Journal of Fluid Mechanics*, Vol. 42, No. 3, 1970, pp. 561–584. https://doi.org/10.1017/S0022112070001489
- [62] Blasius, H., Grenzschichten in Flüssigkeiten mit Kleiner Reibung, Druck von BG Teubner, 1908.
- [63] Goldstein, S., "Concerning Some Solutions of the Boundary Layer Equations in Hydrodynamics," *Mathematical Proceedings of the Cambridge Philosophical Society*, Vol. 26, No. 1, 1930, pp. 1–30. https://doi.org/10.1017/S0305004100014997
- [64] Abramson, H. N., and Ransleben, G. E., "An Experimental Investigation of Flutter of a Fully Submerged Subcavitating Hydrofoil," *Journal of Aircraft*, Vol. 2, No. 5, 1965, pp. 439–442. https://doi.org/10.2514/3.43681
- [65] Schlichting, H., Gersten, K., Krause, E., Oertel, H., and Mayes, K., Boundary-Layer Theory, Vol. 7, Springer, New York, 1955.
- [66] Lighthill, M. J., "On Boundary Layers and Upstream Influence. II. Supersonic Flows without Separation," *Proceedings of the Royal Society of London, Series A: Mathematical, Physical and Engineering Sciences*, Vol. 217, No. 1131, 1953, pp. 478–507.
- [67] Brown, S. N., and Daniels, P. G., "On the Viscous Flow About the Trailing Edge of a Rapidly Oscillating Plate," *Journal of Fluid Mechanics*, Vol. 67, No. 4, 1975, pp. 743–761. https://doi.org/10.1017/S0022112075000584
- [68] Chow, R., and Melnik, R. E., "Numerical Solutions of the Triple-Deck Equations for Laminar Trailing-Edge Stall," *Proceedings of the Fifth International Conference on Numerical Methods in Fluid Dynamics*, Springer, New York, 1976, pp. 135–144.
- [69] Brown, S. N., and Cheng, H. K., "Correlated Unsteady and Steady Laminar Trailing-Edge Flows," *Journal of Fluid Mechanics*, Vol. 108, 1981, pp. 171–183. https://doi.org/10.1017/S0022112081002061

[70] Taha, H., and Rezaei, A. S., "Unsteady Viscous Lift Frequency Response Using the Triple Deck Theory," AIAA Paper 2018-0038, 2018.

- [71] Schlichting, H., and Truckenbrodt, E., Aerodynamics of the Airplane, McGraw-Hill, New York, 1979, p.80.
- [72] Bisplinghoff, R. L., Ashley, H., and Halfman, R. L., Aeroelasticity, Dover, New York, 1996.
- [73] Robinson, A., and Laurmann, J. A., Wing Theory, Cambridge Univ. Press, New York, 1956, pp. 491, 496.
- [74] Taha, H., and Rezaei, A. S., "On the High-Frequency Response of Unsteady Lift and Circulation: A Dynamical Systems Perspective," *Journal of Fluids and Structures*, Vol. 93, 2020, Paper 102868. https://doi.org/10.1016/j.jfluidstructs.2020.102868
- [75] Taha, H., and Rezaei, A. S., "Effect of Viscous Unsteady Aerodynamics on Flutter Calculation," AIAA Paper 2019-2036, 2019.
- [76] Zakaria, M. Y., Al-Haik, M. Y., and Hajj, M. R., "Experimental Analysis of Energy Harvesting from Self-Induced Flutter of a Composite Beam," *Applied Physics Letters*, Vol. 107, No. 2, 2015, Paper 023901. https://doi.org/10.1063/1.4926876
- [77] Billings, S. A., "Identification of Nonlinear Systems—A Survey," *IEE Proceedings D (Control Theory and Applications)*, Vol. 127, No. 6, 1980, pp. 272–285. https://doi.org/10.1049/ip-d.1980.0047
- [78] Haber, R., and Keviczky, L., Nonlinear System Identification-Input-Output Modeling Approach Volume 1: Nonlinear System Parameter Identification, Mathematical Modelling Theory and Applications, Vol. 7, Springer, 1999.
- [79] Giri, F., and Bai, E.-W., Block-Oriented Nonlinear System Identification, Vol. 1, Springer, New York, 2010.
- [80] Taha, H. E., "Geometric Nonlinear Control of the Lift Dynamics of a Pitching-Plunging Wing," AIAA Paper 2020-0824, 2020.
- [81] Taha, H. E., Pla Olea, L., Khalifa, N., Gonzalez, C., and Rezaei, A. S., "Geometric Control Formulation and Averaging Analysis of the Unsteady Aerodynamics of a Wing with Oscillatory Controls," *Journal* of Fluid Mechanics, Vol. 928, 2021.
- [82] Rezaei, A. S., and Taha, H., "Computational Study of Lift Frequency Responses of Pitching Airfoils at Low Reynolds Numbers," AIAA Paper 2017-0716, 2017.
- [83] Rezaei, A. S., and Taha, H., "Circulation Dynamics of Small-Amplitude Pitching Airfoil Undergoing Laminar-to-Turbulent Transition," *Journal* of Fluids and Structures, Vol. 100, 2021, Paper 103177. https://doi.org/10.1016/j.jfluidstructs.2020.103177
- [84] Leishman, J. G., and Beddoes, T. S., "A Semi-Empirical Model for Dynamic Stall," *Journal of the American Helicopter Society*, Vol. 34, No. 3, 1989, pp. 3–17.
- [85] Fung, Y. C., An Introduction to the Theory of Aeroelasticity, Dover, New York, 1969.
- [86] Moore, B., "Principal Component Analysis in Linear Systems: Controllability, Observability, and Model Reduction," *IEEE Transactions on Automatic Control*, Vol. 26, No. 1, 1981, pp. 17–32. https://doi.org/10.1109/TAC.1981.1102568
- [87] Laub, A., Heath, M., Paige, C., and Ward, R., "Computation of System Balancing Transformations and other Applications of Simultaneous Diagonalization Algorithms," *IEEE Transactions on Automatic Con*trol, Vol. 32, No. 2, 1987, pp. 115–122. https://doi.org/10.1109/TAC.1987.1104549
- [88] Kalman, R. E., Ho, Y.-C., and Narendra, K. S., "Controllability of Linear Dynamical Systems," *Contributions to Differential Equations*, Vol. 1, No. 2, 1963, pp. 189–213.

A. R. Jones Associate Editor